THE UNIVERSITY OF MANITOBA

FATIGUE TESTING OF SURGICAL STAINLESS STEEL IN A SIMULATED PHYSIOLOGICAL ENVIRONMENT

by

RICHARD N. HOLTE, B.Sc. (M.E.)

A THESIS

SUBMITTED TO THE FACULTY OF GRADUATE STUDIES

IN PARTIAL FULFILMENT OF THE REQUIREMENTS FOR THE DEGREE

OF MASTER OF SCIENCE

DEPARTMENT OF MECHANICAL ENGINEERING

WINNIPEG, MANITOBA

October, 1976

"FATIGUE TESTING OF SURGICAL STAINLESS STEEL IN A SIMULATED PHYSIOLOGICAL ENVIRONMENT"

by

RICHARD N. HOLTE

A dissertation submitted to the Faculty of Graduate Studies of the University of Manitoba in partial fulfillment of the requirements of the degree of

MASTER OF SCIENCE

Acknowledgements

The assistance of the National Research Council in the form of an operating grant is acknowledged gratefully.

During the preparation of this thesis, I was aided and encouraged by many people. Mr. Wayne Tennese and Mr. Cliff Burton provided much-appreciated technical expertise. Thanks to Miss Karen Read for preparing the final draft, to Miss Burga Kruse for typing the manuscript, and to Mr. Jim Robinson for his help with the graphics.

I count myself fortunate to have worked for Dr. Jack Cahoon. He was a great advisor.

A special note of thanks to Dr. Kris Tangri and Mr. Reinhard Daher.

ABSTRACT

Despite the fact that fatigue failure of 316L stainless steel orthopedic implants is still a problem, it has received scant attention. Tests were performed in air and distilled water, to provide baseline data, and in Ringer's physiological solution, which simulates the extracellular fluid of the body. Results show that the apparent fatigue limit in Ringer's solution is 10% lower than the fatigue limit in air or distilled water which could explain some of the failures in orthopedic implants. A theoretical model based on enhancement of stage I crack growth rates by crevice corrosion is proposed to account for the experimental observations.

TABLE OF CONTENTS

PAGE

List of Figures.

List of Tables.

List of Photographs.

CHAPTER ONE

1. INTRODUCTION

1.1 Historical Background

Metals have been surgically implanted in the human body for many years: in 1562 Petronius used a gold prosthesis to repair a cleft palate (1). Infection was a major problem, however, and early attempts often failed for this reason. The work of Pasteur and Lister in the nineteenth century reduced the possibility of surgical infection, and with the advent of asceptic operations, experimentation with different materials for implanting began in earnest. By 1910, most materials had been eliminated as possible orthopedic supplements for reasons of expense, weakness, or corrosivity. Steels were popular with the surgeons of the day: Lane specified a "stout (high Carbon) steel" (2), while Sherman declared that a new Vandium tool steel was the best available for internal prostheses (3). Thus we see the surgeon searching for a material sufficiently strong and corrosion-resistant for service in the body environment.

In 1926, 18-8 SMo stainless steel was patented (1), and was reviewed by Large (4) as having a good potential as an implantable material. Slow to gain acceptance, in 1947 this steel had been recommended by the American College of Physicians and Surgeons (3) along with Titanium and the Cobalt-based alloy Vitallium, as being suitable for orthopedic repair and supplement. Today these same materials are still effectively and routinely implanted in the body.

1.2 Incidence of Failures

Many clinical surveys of excised orthopedic implants have been done recently. Cahoon and Paxton (5) performed metallurgical examinations

of thirteen failed orthopedic implants and found five to have failed by either a fatigue or a corrosion-fatigue mechanism. They cite poor design and fabrication techniques as major contributory causes. Colangelo (6) and Colangelo and Greene (7) found three fatigue failures in 155 excised implant components. They do not indicate how many of the excised prostheses performed satisfactorily. Brettle and Hughes (8), examining four "apparently random" examples of failed orthopedic implants, report that all of the devices failed by either a fatigue or a corrosion-fatigue mechanism. Of four En58J (British equivalent of AISI 316L) stainless steel implants examined by Hughes and Jordan (9), one had failed due to a corrosion-fatigue mechanism, and another due to a fatigue mechanism, both with failures initiating at section changes. Another study, by Weinstein et. al. (10), reports six of 84 failures attributable to fatigue or corrosion-fatigue.

Failure of orthopedic implants is still a problem, as indicated by the preceeding surveys. Fatigue and corrosion-fatigue account for a significant number of these failures.

1.3 Recent Work

Corrosion of surgical stainless steel in the body has received much attention, both in surveys (Scales, Winter, and Shirley (11, 12), Cohen (13)) and in vitro experiments approximating body conditions (Rama Char (14), Cahoon, Chaturvedi, and Tennese (15)). Considerably less interest has been shown in the fatigue behaviour of 316L stainless steel under simulated body environment conditions.

Laing and O'Donnell (16) conducted static and fatigue tests of several different hip-nail cross-sections machined from rods of

surgical stainless steel. Their work was conducted from a design viewpoint, rather than from a materials selection interest. Consequently, no attempt was made to approximate the harsh environment in which these implants would ultimately find service. On the other hand, Grover (17) dealt with the question of fatigue life of implants from a materials standpoint. He conducted fatigue tests not only of 316L stainless steel but also of Vitallium and a Titanium alloy (Ti-6Al-4V), and prepared S-N curves using the results. Grover's tests were all run in air at room temperature. The possibly detrimental effects of cycling in the warm, moist, chloride environment of the body could not be estimated from his work.

Cohen (18) performed fatigue tests on Sherman plates and surgical nuts and bolts of both Vitallium and 316 stainless steel. His experiment was designed to test relative corrosion rates of the different metals stressed in a saline solution.

Two papers (6, 19) have been published using the fracture mechanics approach to the problem of fatigue in the physiological environment. Wheeler and James (19) showed a distinctly lower crack growth rate in air than under simulated physiological conditions. They chose a sinusoidal forcing function for their baseline (air) tests, but changed to a square waveform for the simulated physiological test. This change in forcing function is regrettable, as it clouds the significance of their results: one is unsure as to how much of the difference between the crack propagation rate in air and that in Ringer's physiological solution is due to the difference in environments, and how much is

attributable to the change in applied waveforms (20). Because of the longer times at peak stress, and the impact loading of every cycle, the square wave is likely to accelerate the rate of crack propagation, precisely the effect that Wheeler and James wish to attribute to the increased harshness of the artificial physiological environment. It seems reasonable to infer that the difference is, at best, not so great as reported in their paper. The other fracture mechanics study, by Colangelo (6), showed a higher crack propagation rate in air than in a saline solution. Curiously, his baseline data do not agree with those of Wheeler and James, despite the generally comparable testing conditions chosen by the respective authors. Commenting on this seeming contradiction, Williams (3) emphasized the statistical nature of fatigue, noting that both authors had tested only one specimen. Brettle concluded that "it seems unreasonable to expect good correlation, or even meaningful results, on the basis of so little data" (21). Colangelo (6) and Wheeler and James (19) have laid the groundwork, showing the range of values that may be expected. Subsequent confirmatory studies are as yet wanting.

1.4 Raison d'être

Surgical stainless steel is widely used for orthopedic repair and supplement. The surveys quoted (5-10) give evidence of significant numbers of in vivo failures by a fatigue mechanism. Work to date (6, 16-19) has left unanswered the possibility of a detrimental effect on fatigue life of repeated loading in the corrosive environment of the body. Both Williams (3) and Brettle (21) have commented on this lack of information available concerning the corrosion-fatigue characteristics

of implant materials. This study will add to the state of the art by investigating the effects of service under physiological conditions on the fatigue behaviour of surgical stainless steel.

2. HUMAN PHYSIOLOGY*

2.1 Body Fluids

The human body is composed of millions of cells, specialized to perform certain functions, and variously aggregated into the macroscopic tissues and organs. Despite their many differences, the cells have several similarities, including the composition of their intracellular fluid, and the metabolic process. The nutrients required for metabolism and the waste products evolved therefrom are transported by extracellular fluid surrounding the cells, which also has a nearly constant composition throughout the body. Extracellular fluid is in constant motion as it transports the nutrients and the waste products between the circulatory system and the cells. Thus the internal environment is a dynamic equilibrium between the intracellular and extracellular fluids, separated by permeable membranes of the cell walls. The temperature is a constant 98.6°F (37°C) throughout.

Extracellular fluid contains quantities of ions of sodium and chlorine, moderate amounts of bicarbonate, and traces of potassium, calcium, magnesium, phosphate, sulfate, and organic acid ions. Blood plasma contains a significant amount of protein, found only in trace quantities in interstitial fluid. Nonelectrolytes, mainly lipids and glucose, make up 60% by weight of interstitial fluid, and 90% of plasma.

Potassium and phosphate are the major constituents of intracellular fluid, with moderate amounts of magnesium and sulfate ions, and only traces of sodium, bicarbonate, and chloride ions present. Additionally, intracellular fluid contains about four times as much

* Note: Most of the information in this section is derived from Guyton's Textbook of Medical Physiology (22), Crouch's Functional Human Anatomy (23), and Basic Physiology and Anatomy by Chaffee and Greisheimer (24).

protein as does blood plasma. Non-electrolytes comprise 97% by weight of intracellular fluid. Figures 1 and 2 give the complete composition of intracellular and extracellular fluids.

Oxygen is required for the metabolic process, and carbon dioxide is a waste product. These gases are present in both intracellular and interstitial fluid, carbon dioxide having a partial pressure of 45 mm Hg in the extracellular fluid and 46 mm Hg in the intracellular fluid, and oxygen having a partial pressure of 40 mm Hg in the extracellular fluid and varying between 0 and 40 mm Hg in the intracellular fluid. These values are subject to variations in available healthy lung surface area, blood composition and flow rate, and basal metabolic rate.

Extracellular fluid normally has a pH of 7.4. The pH of the intracellular fluid has been estimated at between 4.5 and 8.0: Guyton (22) gives 7.0 as an average value.

The composition of the extracellular fluid is closely monitored to protect against any detrimental deviations from the norm. For example, sodium and potassium ion concentrations are regulated by hormones, chiefly aldosterone. Dissolved oxygen and carbon dioxide levels in the blood are monitored by the respiratory centre in the medulla. Variations in pH may be modified by the ubiquitous buffer systems, by regulation of ventilation, and by kidney response.

Despite these elaborate control mechanisms, deviations from the norm do occur, especially with traumas. Upon injury, histamine is liberated by damaged cells, increasing the local blood flow and permeability of capillaries. Large quantities of fluid and protein infuse the area,

and clotting of the extracellular and lymphatic fluids takes place. This closure of the injured area prevents the spread of any foreign bacteria that may be present, and reduces fluid flow to a very low level. This brings a rise in the local pCO_2, and a decrease in the pO_2. Local pH may drop as low as 5.5, and remain thus for ten days, before slowly returning to the normal level (Murray (25), Crimmins (26), Laing (27)).

The intra- and extracellular fluids, and the ions and gases dissolved in them, are the basic internal environment of the body. Numerous effective monitoring and regulatory mechanisms maintain a steady state composition of these dynamic fluids. Deviations from the norm occur locally upon trauma.

2.2 Nerves

Neurons are cells which have specialized to conduct electrochemical impulses through the body. They vary in length from a fraction of an inch to several feet. Basically, neurons consist of a cell body with elongated processes, known as nerve fibres. Dendrites are nerve fibres which receive impulses and transmit them toward the cell body, while axons carry impulses away. Neurons have only one axon, although it may throw off collateral branches. Axons and dendrites may develop sheaths of myelin and neurilemma. Myelin is an excellant insulator, but its sheaths are discontinuous, being periodically interrupted at constrictions known as nodes of Ranvier. Neurilemma sheaths are found on all nerves outside the central nervous system. They protect the nerve fibres, are much better conductors than myelin sheaths, and play an important role in the regrowth of severed nerve fibres.

An electrical potential of -85 mv exists between the extracellular fluid and the intracellular fluid of nerve fibres. This is known as the normal resting potential, and results form the action of the sodium and potassium ion pump within the nerve fibre membrane, and the selective permeability of the membrane. Potassium diffuses through the resting nerve membrane 50 to 100 times more easily than sodium.

The transmission of nerve impulses is initiated by a sudden increase in the permeability of the membrane to sodium ions, thought to be caused by the emigration of calcium ions. The great difference of sodium ion concentrations across the cell wall causes a large influx of these ions into the cell, temporarily making the intracellular fluid 50 mv positive with respect to the extracellular fluid. This provides a repulsive force to stop the flow of sodium ions into the nerve fibre. At this time the membrane appears to resume its former impermeability to sodium ions, while allowing potassium ions to diffuse at 30 to 40 times their former rate. The conjoint action of the sodium pump and the increased potassium diffusion results in an excess of cations in the extracellular fluid immediately adjacent to this portion of the nerve fibre. This cation excess is characterized by a positive after potential of -90 mv. As the membrane permeability to potassium ions returns to normal, the potential slowly resumes its normal resting value. On a time scale, the peak reversal or action potential is achieved in about .5 milliseconds, the positive after potential follows in another 8 milliseconds, and the resting potential is regained no sooner than 50 milliseconds and as long as several seconds after the initial change in sodium ion permeability in

the nerve fibre membrane. The electric current that accompanies the moving ions is thought to stimulate this change in permeability in neighbouring cells. Thus conduction of a nerve impulse is a self-sustaining propagation: the moving ions cause a current which changes the permeability of the neighbouring membrane, starting the depolarization of the adjacent portion of the nerve fibre, and propagating the impulse further. A threshold level of stimulation is required to initiate depolarization. Conduction may occur in all directions along the nerve fibres. There is an absolute refractory period of 1/2500 of a second during which no amount of stimulation will cause depolarization of the nerve fibre. The velocity of conduction varies from 2 to 400 feet/second, the higher values being typical of saltatory conduction in myelinated fibres which depolarize only at the nodes of Ranvier, thus lengthening the jumps of each depolarization process.

Nerve fibres have a resting potential of -85 mv. The conduction of a nerve impulse raises this briefly to +50 mv, from where it drops quickly to -90 mv, and then slowly returns to the normal resting potential. Ion exchange across the nerve fibre membrane play an integral part in impulse propagation.

2.3 Bones

The bones of the skeleton are the structural framework of the body. They give the body shape, act as levers in the transmission of force generated by the muscles, protect softer interior tissues and organs, and act as a storehouse and supplier of various organic and inorganic compounds. Structurally, a bone consists of a matrix of cancellous (spongy) bone surrounded by a dense layer of compact bone. Periosteum forms the majority of the outer covering.

Bone is composed of a tough organic matrix that is greatly strengthened by deposits of crystalline salts. Collagen fibres, comprising 97% of the organic material, have good tensile strength, and tend to grow along the lines of tensional stress. The crystalline salts, mainly hydroxyapatites of calcium and phosphate, are strong in compression. Intimate contact of the collagen fibres and the inorganic salts, and cross-bonding of collagen fibres, makes bone strong in tension, compression, and shear. Morral (28) gives the ultimate strengths of femur bone as 13 to 17.7 ksi in tension and 18 to 24 ksi in compression, with a Young's modulus of from 2.82 to 2.98 psi x 10^6. These figures are subject to variations of age, sex, and racial type: men have stronger bones than women, Negroes more so than Caucasians (29). Furthermore, as a person ages, the mineral salts replace the collagen fibres, decreasing the organic content of bone below its normal 30%, and resulting in decreased strength and increased brittleness.

Because bone is a living, growing tissue, it reacts to external stimuli. Through the action of osteoclasts and osteoblasts, bone is continually resorped and replaced. In this way, bones optimize their structure to accomodate the loads they must carry. The action of the bone-altering cells is thought to be guided by piezoelectric current generated by the compression of bone. Other authors (26, 30) have commented on this effect, but it has yet to be measured quantitatively.

Marrow is found in the hollow shafts of the long bones and within the cavities of cancellous bone. Red marrow produces red and white blood cells and platelets, and is responsible for the destruction

of old worn-out cells through phagocytosis. Consequently, the marrow communicates freely with the circulatory system. This rich blood supply also connects to the haversian system and canaliculi of the bone, supplying nutrients and removing metabolic wastes. Through this contact with the circulatory system, inorganic salts may be deposited in or removed from the bones, depending on the particular needs of the body as determined by the person's activities and nutrient intake.

The bones provide a framework for the body. They are able to modify their structure in response to the differing loads they are required to carry. Many organic and inorganic compounds are either stored in the bones, or manufactured there. Because of this, bones play a dynamic role in the maintenance of normal body fluid composition. Variations in strength of bone tissue occur particularly with advancing age, as the organic fibres are replaced with inorganic salts, rendering the bones weaker and more brittle.

2.4 Skeletal Muscles

The skeletal muscles, which account for 40% of the body weight, produce all of the voluntary movements. The muscles consist of many muscle fibres running the length of the muscle, innervated usually at one point only. The muscle fibres, of diameter 10 to 100 microns, are in turn made up of from 100 to several thousand myofibrils, suspended in a sarcoplasm matrix. Each myofibril is composed of about 1500 myosin filaments and twice as many actin filaments, Matrices of myosin filaments interdigitate with matrices of actin filaments, which are cross linked at their centre points by Z membranes. Thus the motor units, or sarcomeres, are found between adjacent Z membranes.

Muscular contractions originate at the myosin and actin filament level. The normal muscle resting potential of -85 mv is excited to +100 mv by an electrochemical nerve impulse of duration 5 to 10 milliseconds, transmitted from the nerve to the motor point of the muscle and thence to all of the myosin and actin filaments by way of T tubules that permeate the entire muscle. The excitation potential is thought to cause, in conjunction with calcium ions and ATP, an electrical attraction along the myosin fibrils and sliding together and overlapping of the associated actin fibrils. The conjugate action of the slight shortening of all of the sarcomeres results in a macroscopic contraction of the muscle. Force and duration of contraction are affected by the number of muscle fibres stimulated, and the frequency of stimulation.

Muscular contractions are the macroscopic manifestations of a microscopic electrochemical reaction. Stimulation by a nerve impulse briefly depolarizes the normal muscle resting potential of -85 mv to +100 mv.

2.5 Modelling the Body Environment

The chemical composition of the extracellular fluid, noted in Figure 1, is closely approximated by Ringer's physiological solution (Table 1). The dissolved gas partial pressure of both oxygen and carbon dioxide is roughly 40 mm Hg. Extracellular fluid normally has a pH of 7.4, although this may drop as low as 5.5 during the initial post-trauma period.

Body temperature is essentially constant at 98.6°F (37°C).

Electrical impulses originating in muscle or nerve cells briefly change the normal resting potential from -85 mv to as much as +100 mv. The piezoelectric properties of bone have not been determined quantitatively. Modelling these various electrical signals will not be necessary, however, as the difference in rest and breakdown potentials for 316L stainless steel in a physiological environment is five times greater than the magnitude of the normal resting potential (15).

Bones of the leg have an ultimate tensile strength of approximately 15 ksi. Because of restrictions of size, geometry, and stress concentrations inherent in fastening, orthopedic implants are subjected to much higher peak stresses. Furthermore, these stresses are applied often: level walking at 51 cpm (31) is repeated many hundreds of times daily.

Surgical stainless steel implants are subject to high stress, low frequency fatigue in a warm, aggressive environment. Electrical impulses associated with nerve and muscle activity are likely insignificant in magnitude, and can be ignored in modelling.

3. EXPERIMENTAL APPARATUS AND PROCEDURE

3.1 Philosophy of Testing

It was anticipated that stressing in the aggressive simulated body fluids would result in lower fatigue life than would be predicted in air under the same loading conditions. This could be verified by constructing S-N curves based on tests run in 37°C air and under simulated body conditions. As a further comparison, tests would be performed using distilled water rather than simulated physiological fluid as the testing medium. In this way, the effect of the aggressive physiological environment on fatigue life of 316L stainless steel could be isolated and identified.

3.2 Specimen Preparation

Specimens were lathed from half-inch diameter 316L rod. Uniform surface finish was ensured by consecutive polishing with 200, 400 and 600 grit emery papers. Finished specimens had a diameter of .138 inch and an overall length of 2.25 inch. Just prior to testing, the specimens were degreased in trichlorethylene, washed in hot water, rinsed in cold water and ethanol, and dried under a hot-air blower. Specimen configuration and dimensions are given in Figure 3.

3.3 Apparatus

Fatigue tests were performed on an Amsler high-frequency Vibraphore (Photo 1), type HFP22, fitted with a two-ton optical dynamometer. The specimens were axially loaded form zero to peak tensile stress (stress ratio, R = 0) at approximately 8500 cpm, the forcing function being sinusoidal in nature. Failure criterion was complete fracture, with run-out at five million cycles.

To accomodate the different environments, a seven-inch cube of UPVC with removable lid and 'O' ring seal was constructed (Photo 2). Adaptors of one inch diameter type 304 stainless steel (Figure 4) held the specimens in place in the environmental cell. Initially, the adaptors were accorded the same cleaning treatment as previously described for the specimens. The environmental cell and heating chamber were sterilized with a .2 N HCl solution, washed with soap and warm water, rinsed in warm and cold water, and air-dried. When the different testing media were changed, this procedure was repeated, and fresh distilled water was allowed to circulate for 30 minutes before being drained off.

The temperature of all tests was $37 \pm \frac{1}{2}^{\circ}$ C. A Yellow Springs Instrument Co. Model 63 RC (Photo 3) relay, used in combination with either a T2900 or T2930 thermoprobe, monitored the temperature of the medium in the environmental cell. Heating of the air was performed by an Oster air blower (Photo 4), whereas the liquids were warmed in a separate chamber by a Briskeat heater, and circulated through PVC tubing by a Manostatic Veristaltic Junior model peristaltic pump delivering .3 litre/min.

Distilled water for use as a testing medium and in preparation of Ringer's physiological solution was prepared by passing tap water through a Pako Super Life Water Filter and distilling it in a glass, single-pass Corning AG-1b distillation unit.

For the tests done in an aqueous or physiological environment, commercial purity argon, oxygen, and carbon dioxide were bubbled through airstones placed in the heating chamber (Photo 5). A PHM-71 Acid-Base

Analyzer with pO_2 and pCO_2 modules was used to measure gas partial pressures and acidity of the circulating fluid. Leads to the pO_2 and pCO_2 electrodes were attached directly to the environmental cell, to enable continuous monitoring of these parameters (Photo 6). Both oxygen and carbon dioxide partial pressures were kept at 40 $\pm$ 20 mm Hg. Solution discharging from the electrodes was collected in a 125 ml Erlenmyer flask, and pH checked intermittantly before successive voidings of the flask.

The aqueous and simulated physiological environment media were constantly replenished as evaporation and leakage depleted the circulating fluid. Complete changes of fluid were as far apart as twelve days, and as frequent as two days.

All tests were conducted in an air-conditioned laboratory, with an average temperature of 22 $\pm$ 2°C and a relative humidity of 25 $\pm$ 7% as determined by sling psychrometer.

3.4 Procedure

3.4.1 Tests in a Liquid Environment

The fluid was introduced into the heating chamber, and warmed to the required temperature. Simultaneously, the water bathing the pO_2 and pCO_2 electrodes was heated.

Corrected barometric pressure was calculated, and the pO_2, pCO_2, and pH units were calibrated using gases and buffer solutions of known composition.

The specimen was cleaned as previously described (3.3), and secured in the testing configuration (Photo 2). Plastic tubing was connected, fluid flow initiated, and bubbling of argon and carbon dioxide through the airstones in the heating chamber was begun.

Mean stress level was set on the Amsler Vibraphore. When favorable dissolved gas content and temperature were achieved in the fluid, which usually took about two hours, the alternating stress component was actuated. Load levels and pO_2, pCO_2 and pH of the fluid were monitored throughout the test.

Upon completion of the test, the fluid was siphoned from the environmental cell, the Amsler cross-head raised, and the fractured specimen removed. After drying, it was placed in a labelled envelope and stored in a desiccator.

3.4.2 Tests in Air

The specimen was cleaned, and placed in the testing configuration. Warmed air was allowed to circulate through the environmental cell for about 15 minutes before the alternating loads were applied. Upon completion of the test, the fractured specimen was placed in a labelled envelope and stored in a dessecator. Applied loads were monitored during the test, as were relative humidity and temperature of the room air as determined by sling psychrometer.

CHAPTER FOUR

4. RESULTS

4.1 Material Tests

4.1.1 Chemical Composition

The stainless steel rod was sectioned and cold-rolled to a 1/8 inch thick x 3/4" wide bar. This was mounted in bakelite, and polished with 100, 200, 400, and 600 grit emery papers. The unknown sample and a similarily-prepared standard of known composition were placed in the specimen holders of a Philips Norelco flourescence analysis machine. The X-rays were excited at 35 kv and 20 ma. Threshold and window voltage levels on the counter were kept constant at 18 and 15 volts respectively. After the angle of bombardment and counter voltage had been chosen for a particular element, pulses were counted for a ten-second interval, and noted. Background radiation ("noise") was determined by taking counts at one degree above and below the angle detecting maximum intensity of counts. Experimental data follows.

Element: Chromium

Counter voltage = 1062 v ϕ = 69.2°

Number of counts, 10 second interval:

	Standard	Background	Unknown
	113.	1° high 2	113.
	113.	1° low 1	117.
	110.		121.
	113.		114.
	113.		112.
	112.		117.
Averages:	112.3	1.5	115.7

Content of standard: 17.25%

Content of unknown: $\frac{17.25}{100} \times \frac{(115.7 - 1.5)}{(112.3 - 1.5)} = 17.78\%$

Element: Nickel

Counter Voltage = 1056 v $\emptyset$ = 48.6°

Number of counts, 10 second interval:

	Standard	Background	Unknown
	351.	1° high 22	364.
	354.	1° low 33	347.
	351.		348.
	367.		359.
	351.		368.
	361.		348.
Averages:	355.8	27.5	355.7

Content of standard: 12.5%

Content of unknown: $\frac{12.5}{100} \times \frac{(355.7 - 27.5)}{355.8 - 27.5} = 12.5\%$

Element: Molybdenum

Counter voltage: = 925 v $\quad \emptyset = 20.38°$

Number of counts, 10 second interval:

Standard	Background	Unknown
258.	1° high 53	231.
252.	1° low 76	220.
254.		220.
258.		228.
254.		221.
264.		227.
Averages: 255.0	64.5	224.5

Content of standard: 2.33%

Content of unknown: $\frac{2.33}{100} \times \frac{(224.5 - 64.5)}{(255.0 - 64.5)} = 1.96\%$

Element: Manganese

Counter voltage = 1050 v ϕ = 62.9°

Number of counts, 10 second interval:

Standard	Background	Unknown
20.	1° high 4	23.
23.	1° low 10	24.
18.		22.
19.		23.
21.		24.
20.		23.
Averages: 20.2	7.	23.2

Content of standard: 1.4%

Content of unknown: $\frac{1.4}{100} \times \frac{(23.2 - 7.)}{(20.2 - 7.)} = 1.7\%$

A 30 gm sample of lathe turnings was sent to Warnock - Hersey Professional Services Ltd. to determine the carbon content. It was found that the sample contained .04% carbon by weight.

4.1.2 Mechanical Properties

An Instron testing machine was used to determine the mechanical properties. Specimens (Figure 5) were machined from half-inch rod stock as previously described (3.2). A total of eight experiments were performed, four each in air and Ringer's physiological solution.

After the Instron was zeroed and calibrated, tests were begun, using a crosshead speed of .2 cm/min. Load and extension were recorded on a built-in X-Y plotter moving at 2 cm/min. Specimen preparation and control of environment were the same as for the fatigue tests. Ultimate tensile load and elongation were read directly from the load-extension plot, and .02% offset yield load was derived form the graph also. Reduction in area was estimated by using a Hounsfield area reduction gauge.

Except for the elongation, where specimens averaged 64.33% in Ringer's solution versus 54.75% in air, there was little difference in the results of tests conducted in the two media. Yield strength averaged 72,443 psi and ultimate tensile strength averaged 87,987 psi, with an average reduction in area of 75.88%. Tables 2 and 3 give complete experimental data.

4.1.3 Microstructure

Fractured samples 33, 57, 61, 71, and 77 were sectioned in the threads and mounted in bakelite. Polishing on 100, 200, 400, and 600 grit emery papers, and with Linde 6 μ polishing solution left a mirror finish. After etching for 20 seconds in a solution of equal parts glycerine and nitric and hydrochloric acids, the mounted specimens were examined at 100 x magnification. Pictures (Photos 7 - 11) were taken,

and grain size estimated. Average grain size was ASTM 5.5 - 6. A single phase was noted throughout. No porosity was evident. Very few inclusions were found.

4.1.4 Hardness

Specimens 23, 33, 61, 71 and 77, mounted in bakelite as above, were tested on a Vicker's hardness testing machine using a 10 Kg. load. Average hardness was DPH 200.

4.2 Fatigue Tests

Results of the fatigue tests are presented graphically (Figures 6, 7, 8 and 9) and in tabular form (Tables 4, 5 and 6).

4.3 Statistical Analysis of Fatigue Data

4.3.1 Application of Chauvenet's Criterion

The data was organized into groups according to maximum alternating stress applied and testing medium. Mean life, $\bar{x}$, and estimate of standard deviation, s, were calculated for each data group. Chauvenet's criterion, based on the probability of finding one element of a normally-distributed population more than 1.96 standard deviations away form the mean (which corresponds to a 95% confidence limit), was selected to determine the reliability of certain outlying data points. A measure of dispersion, c, can be calculated as:

$$c = (x_e - x)/s \quad \ldots \text{ from (32)}$$

where $\bar{x}$ and s are as described previously and x_e is the life of an element in a data grouping. If c exceeds the value of c', where c' is the probability of finding x_e at 1.96 s from $\bar{x}$, the element in question can be rejected from the data group with 95% confidence.

The test as described was applied (Table 7) to the data groups deemed most likely to be affected. Only one grouping was altered, the specimens tested in air with stresses alternating between zero and 76 ksi, where test number 66 (life of 800 kc) was removed.

4.3.2 Application of Student's t Test

This test is a well-known method for checking for the existence of a statistically significant difference between the means of two normally-distributed populations. Application of this criterion revealed that at the 80 ksi stress level, statistically significant differences were found between experiments performed in air and Ringer's solution (99% confidence) and between tests conducted in Ringer's solution and distilled water (95% confidence). The lack of statistical significance to the apparent differences found at lower stress levels is attributable to the greater dispersion and fewer number of tests conducted at those levels.

Table 8 gives the results of the statistical analyses of the experimental data.

4.4 Verification of Fatigue-testing Machine

In accordance with the recommendation of the Amsler Co. (33) that the Vibraphore be calibrated every six months during periods of constant use, the machine was checked for inaccuracy in indicated loads after the completion of the testing sequence.

A load cell was constructed by mounting four identical 1/4 inch strain gauge (gauge factor 2.05) on an adaptor. Two of the strain gauges were oriented along the longitudinal axis of the adaptor, and two along the transverse, with one gauge of each respective orientation

on opposite sides of the adaptor. Leads were attached, and a full bridge circuit was constructed. An Automatic Industries model SB-I switch and balance unit and a model 350 strain indicator completed the load cell. The load cell was calibrated on an Instron universal testing machine, which was in turn calibrated electronically.

The load cell was connected to the Amsler Vibraphore and static loads of zero to 1200 pounds were applied in 200 pound increments. For the range of loads employed during the fatigue testing indicated loads were 2.5 to 2.6% below true loads. Complete results are given in Tables 9-A and 9-B.

CHAPTER FIVE

5. DISCUSSION OF RESULTS

5.1 Material Properties

5.1.1 Chemical Composition

Table 10 lists the ASTM composition requirements, and the composition of the experimental material. The stainless steel that was used falls within the accepted limits of composition, except for molybdenum and carbon. The carbon content (.04 weight %) is above the maximum allowable content for surgical stainless steel (.03 weight %), and the molybdenum content is slightly below (1.96 weight %) the required content (2. - 3. weight %). Because the Philips fluoresence analyzer is accurate only to $\pm$ 5%, the molybdenum content may well be within the required limits. The effect of these compositional deviations will be to increase the tendency to form chromium carbides, and thus lower the corrosion resistance of the metal. Because the chromium content is above the minimum required (17.78 versus 17.0 weight %), this effect will likely be small.

5.1.2 Mechanical Properties

The average hardness of the five specimens tested was DPH 200, indicating an almost fully-annealled state. ASTM (33) requires fully-annealled 316L stainless steel to have a yield strength of at least 25 ksi, and ultimate tensile strength of 70 ksi, and a minimum elongation of 40%. The experimental stock surpassed all of these requirements, having a .02% yield strength of 72 ksi, an ultimate strength of 88 ksi, and an elongation of 59%.

Note that strength and ductility were virtually identical for tests run in air and in Ringer's physiological solution.

5.1.3 Microstructure

Average grain size of the specimens was ASTM 5.5 - 6., within the requirement of grain size 5.0 or finer (35).

The material was noted to be single-phase throughout. This is important, as galvanic corrosion often occurs in metals containing two or more phases.

Stainless steel for surgical implants is required (35) to have a low inclusion count, and it can be seen from the photomicrographs (Photos 7 - 11) that this condition has been satisfied by the material used in the present study.

5.2 Statistical Analysis

Applying Student's t test to the different fatigue data groups revealed that at the 80 ksi stress level a statistically significant difference at the 99% confidence level existed between the tests run in Ringer's solution and those run in air, and a significant difference (95% confidence) was also found between the tests conducted in a distilled water environment and those performed in Ringer's physiological solution. The increased scatter and low number of tests would account for the fact that similar differences were not noted at lower stress levels.

5.3 Phenomenonological Approach to Corrosion Fatigue

5.3.1 At High Stresses

Cycling a ferrous metal in a corrosive medium modifies the well-known shape of a "dry" S-N curve (36, 37, 38). As the environment becomes increasingly hostile, the S-N curve shifts further to the left, signifying a reduction in life at a given stress. This tendency was

noted in the present study: fatigue life in Ringer's solution was shorter than in distilled water, which was in turn shorter than in air. Investigations based on the fracture mechanics approach to corrosion fatigue show that in this high stress region, crack propagation proceeds at about the same rate, regardless of testing medium (6, 19, 39). This indicates that the decreased life of specimens tested in a corrosive environment is due to an enhancement of the crack initiation rate by the corrosive medium. The frequency at which the loads were applied also affects the fatigue life of the specimens (40). Higher frequencies of testing tend to shift the S-N curve to the right (longer life), due to less time in contact with the corrosive medium for a given number of cycles, and hence less environmentally-induced damage to the test specimen. Results of this study are consistent with these considerations: in the limiting case, the tensile tests conducted in both air and Ringer's physiological solution had equivalent results.

5.3.2 At low stresses

The difference between the air and corrosive atmosphere tests is even greater at low stresses (36, 37, 38). In this stress region, the corrosion fatigue curve shifts to the left and the sharp "knee" at the fatigue limit becomes rounded as the curve gradually tapers to the right, asymptotically approaching an apparent fatigue limit at about 10^7 cycles that is below the true fatigue limit characteristic of ferrous metals (Figure 10). As the environment becomes increasingly hostile, these changes are more marked.

The results of this present study are in general agreement with the classical observations of corrosion fatigue. As the testing

environment became more corrosive, specimen life at any given stress level decreased. An apparent fatigue limit was observed in Ringer's solution that is clearly lower (10%) than the true fatigue limit. Contrary to expectations, experiments conducted in water showed a fatigue limit similar to that of tests run in air. This may be due to the fact that the small (with respect to 316L stainless steel) corrosivity of water is further reduced by the high frequency of load application. Nonetheless, it is reasonable to expect a difference between the fatigue limit and the apparent fatigue limit for tests conducted in water; and it is unfortunate that more experiments under these conditions were not performed.

At low stresses, crack propagation is usually found to be more rapid in corrosive than in non-corrosive environments (19, 39). However, since over 90% of specimen life in high cycle fatigue is required to initiate a critical-length stage 1 crack (45) the effect of environmental enhancement of crack growth rates is likely more important in the initiation and stage 1 propagation aspects of crack growth.

5.4 Theoretical Model for Corrosion Fatigue of 316L Stainless Steel in a Simulated Physiological Fluid

There are many theories that attempt to explain the phenomena of corrosion fatigue. Laird and Duquette (41) have commented on the inadequacy of all of these models in universal applications, and Karpenko has gone so far as to suggest that different mechanisms operate at different stress levels (42). Accordingly, the model that is based on the preferred dissolution by the corrosive medium of cyclically deformed

areas of the metal has been modified to explain the behaviour of 316L stainless steel as reported in this paper.

Fatigue cracks grow in three stages (43). In the first stage, a notch is initiated, either due to slip of cyclically deformed areas of the metal (e.g. persistant slip bands) or orginating from an inclusion or other fabrication flaw. The notch acts as a stress-raiser, and stage 1 crack propagation begins. In the second stage of crack growth, shear is the operating mechanism, and growth is on a plane favorably oriented for shear. Continued growth of a stage 1 crack reduces the effective cross section of the material, raising the net section stresses. Stage 2 propagation follows, with the crack growth being perpendicular to the axis of applied stress. Fracture of the member occurs when the stresses in the uncracked portion exceed the ultimate tensile strength of the material.

The present theory is concerned with the enhancement of initiation and stage 1 propagation through environmental action. Basically, various surface discontinuities are available to act as sites for the crevice corrosion of the metal in saline solution. This localized attack is particularly important in the formation of a notch and the growth to a critical size of a stage 1 crack. At lower stresses, surface deformation is not great enough to facilitate crevice corrosion, and an apparent fatigue limit is reached.

5.4.1 At high stresses

The combination of high stresses and geometrical constraints causes the puckering of grain boundaries, forming notches that are preferred

sites for crack initiation (41). Laird and Krause (44) simulated this effect with plasticine, and found that grain boundary notches are formed quickly after the onset of high-stress cyclic loading.

Although the surface of the stainless steel is protected by a Cr_2O_3 film, the sides of the notch are freshly-exposed, and therefore not similarily protected. In the notch (or crevice) iron is oxidized, and oxygen is reduced to hydroxide ions until the local oxygen supply has been depleted. In the tip of the crevice, iron dissolution continues unaccompanied by the reduction reaction, resulting in an excess of metal cations which attracts Cl- anions. The ferrous chloride combines with water to form an insoluble hydroxide of iron, and a free acid, H^+Cl^-, which accelerates the further dissolution of iron in the crevice tip. As more iron is oxidized, more Cl^- ions are attracted, and the damage to the metal intensifies (36).

The suseptibility of stainless steels to crevice corrosion in saline solution is well-known. At high stresses, grain boundary notches are preferred sites for initiation of crevice corrosion attack. These notches may be large enough that stage 1 propagation enhanced by crevice corrosion can begin immediately. It is further proposed that the propagation of a stage 2 crack proceeds so quickly due to the high applied stresses (and particularily with low cycle - high frequency corrosion fatigue) that the effect of the environment is rather small in comparison for this particular stage of crack growth.

This model accounts for the behaviour of 316L stainless steel as reported in this paper. Tests conducted in air were not subject to

the corrosivity of the Ringer's solution, and so longer life as a result of the delay in crack nucleation and stage 1 propagation was observed. Applying the model to the tests performed using a distilled water environment, note that aerated water aids in the removal of some surface metal ions. The crevice corrosion process is incomplete because no Cl^- anions are present. The corrosion process in distilled water may end at this point, due to concentration polarization, or may assume the form of a differential aeration cell, which will proceed more slowly than the crevice corrosion associated with the presence of Cl^- ions, because oxygen is less powerful than chlorine as an oxidizer. Regardless of which mechanism is operating, the environmental enhancement of initiation and stage 1 crack propagation is less in distilled water than in Ringer's solution, but greater than in air, which explains why specimens tested in water showed lives intermediate to those loaded in the other media.

5.4.2 At low Stresses

Crack propagation investigations using the fracture mechanics approach to the problem of corrosion fatigue usually show that cracks will propagate more quickly in a corrosive than in a non-corrosive medium (19, 39). However, since notch formation and stage 1 growth require about 97% (45) of specimen life, it is obvious that the large disparities between fatigue and corrosion fatigue lives at medium and low stresses must be due primarily to an effective enhancement of the initiation process by the corrosive environment, a process which ceases to operate below the apparent fatigue limit of the metal-environment combination.

There are two factors which are essential to the continuing operation of any corrosion fatigue mechanism (43):

1. the creation of new surfaces, resulting from either mechanical or chemical action; and
2. the transport to the active corrosion site of environmental agents participating in the chemical reaction.

From the fracture mechanics studies, in which the effect of the environment is evident throughout crack growth, it can be concluded that diffusion to the crack tip is not the limiting factor, especially since stage 1 cracks are much shorter than the stage 2 cracks considered in those papers. The passive behaviour of 316L stainless steel in Ringer's solution eliminates chemical action as the sole agent for creating new metal surfaces, leaving mechanical damage due to fatigue as responsible for exposing unprotected areas of metal in a configuration suitable for the onset of crevice corrosion.

Notches due to grain boundary puckering, discussed earlier in this paper, are a low-cycle fatigue phenomenon. Laird and Smith (45) have commented on the coexistence of grain boundary notches and persistent slip bands and associated formations at high stresses, and Porter and Levy (46) and Kemsley (47) have noted the transition of fracture initiation mode from intergranular to transgranular (grain boundary notches to slip bands) at intermediate stresses. These authors (46, 47) also observed that all high-cycle fatigue cracks originated in persistant slip bands. Clearly, persistant slip bands are increasingly favored crack initiation sites as stresses are reduced from the low-cycle fatigue level.

Holes (48), extrusions and intrusions (45, 49), and notch-peak surface discontinuities (50) are found in persistant slip bands. These various topographic irregularities grow gradually to a critical size at which, in fatigue, stage 2 cracks begin to propagate. Assume that there is a minimum notch depth at which stagnation and thence crevice corrosion can occur, and notice from the behaviour of grain boundary notches at higher stress fatigue that this minimum crack length for crevice corrosion is less than the length necessary for stage 2 crack propagation to begin in air. Accordingly, stage 2 propagation will begin more quickly under corrosive than non-corrosive conditions, resulting in the decreased fatigue life observed in Ringer's solution, and to a lesser extent in distilled water. This model also explains the existence of an apparent fatigue limit, and why it is lower than the true fatigue limit. Below the fatigue limit, stage 1 cracks terminating due to work-hardening of the adjacent crystal will not be long enough to raise the net section stress sufficiently to invoke the transition to stage 2 propagation, but will be greater than the critical length required for the initiation of crevice corrosion. Thus corrosive action will begin, and the corrosion-fatigue specimen will show a finite life. At even lower stresses, stage 1 cracks will terminate shorter than the critical length required for crevice corrosion, and an apparent fatigue limit will be reached. Because the corrosivity of distilled water is not as great as that of Ringer's physiological solution, these effects will be less noticeable in this medium.

5.5 Application to Implant Design

Because the frequency at which the experimental specimens were loaded is well above that which implants would encounter in the body (31), a comment on frequency effects is appropriate.

Endo and Miyas (40) investigated the effect of different cycling frequencies on the fatigue life of mild steel in both tap water and saline solution. They found that at a given stress level, increased frequency tended to lengthen the life of a specimen. This is due to the decreased time of exposure to the corrosive medium, and hence less damage to the specimen after a given number of cycles, and is consistent with both the observed behaviour of materials and the proposed model for crack initiation and propagation. Although their tests conducted in saline showed no fatigue limit, those experiments performed in water did tend towards a fatigue limit which, after 10^7 cycles, was slightly lower for the lower frequency than for the higher.

Marcus and co-workers , (51), using the fracture mechanics approach to the corrosion fatigue of 2024-T3 Alclad aluminum in dry and humid air, noted a decrease in crack propagation rate with increased frequency in both environments. This is consistent with the earlier findings of Endo and Miyas, who constructed S-N curves from their results.

The present programme of experiments revealed a significant decrease in fatigue life above the apparent fatigue limit for 316L stainless steel when a physiological environment rather than room air was employed as the testing medium. This difference would almost certainly be even greater for cycling at the low frequency characteristic of human locomotion.

The fatigue limit of surgical stainless steel decreased 10% when it was cycled in simulated physiological environment. This decrease is similar to the one noted by Endo and Miyas (40) for mild steel tested in tap water. Hence it is reasonable to infer that the experimentally determined reduced fatigue limit is a good approximation of the fatigue limit that would have been observed had the specimens been cycled at a frequency closer to that of human locomotion.

Corrosion fatigue experiments were conducted in air, distilled water, and Ringer's physiological fluid, at a frequency much higher than is typical of the cyclic loading of human locomotion. The purpose of this paper was to determine the performance of surgical stainless steel in orthopedic implants, and one of the established conditions of that type of service is a relatively low frequency of loading (51 cpm (31)). The decrease in fatigue life at stresses greater than the fatigue limit will likely be even greater in the body than as found experimentally, but the fatigue limit in artificial physiological fluid is a good approximation of what can be expected under the in vitro conditions.

The real significance of the reduced fatigue life of an implant can best be understood with reference to the actual experience with orthopedic supplements. The surveys quoted earlier in this paper (5-10) cite examples of implants under-designed for the loads they must bear. The results of this paper show that an orthopedic implant can be designed properly for service under non-corrosive conditions (room air), yet have a limited fatigue life expectancy in the in vitro environment due to the harshness of the extracellular fluid. Although this study

does not delineate the precise nature of the S-N curve that is characteristic of 316L stainless steel loaded in vitro (because of the high frequency of cyclic stressing used in the experimental tests), it does give a good idea of the fatigue limit that can be expected of this material under these conditions. Most stainless steel orthopedic appliances are used to assist the elderly (3, 12). Because there is no way of knowing how many years of service will be required of the implant, nor is it desireable to subject an elderly person to the severe trauma accompanying an operation for the removal of an orthopedic device, it is best to design implants for infinite life. In this application, the present study is valuable, for it shows what fatigue limit can be expected of 316L stainless steel in the physiological environment.

CHAPTER SIX

6. CONCLUSIONS

1. At any given stress level above the apparent fatigue limit, the fatigue life of 316L stainless steel was increasingly reduced as the corrosivity of the environment increased. The apparent fatigue limit in Ringer's physiological (60 ksi) solution was 10% below the fatigue limit in air (66.7 ksi).
2. This reduction in life could account for many of the failures encountered with 316L stainless steel orthopedic implants which were designed using fatigue data gathered in air.
3. The theoretical model for corrosion fatigue of 316L stainless steel explains the experimentally observed behaviour of this metal in all of the environments in which it was tested. However, this is an inferred model rather than an observed phenomena. It is suggested that further experiments be performed to validate the proposed mechanism of corrosion-fatigue.

Table 1. Modelling the Physiological Environment.

PARAMETER	BODY	EXPERIMENT
Temperature (°C)	37.	37.
Extracellular Fluid (meq/l*)		Ringer's Solution:
Na^{+}	132. - 150	138.
Cl^{-}	100. - 110.	114.
HCO_3^{-}	24. - 30.	29.
Ca^{++}	4.5 - 5.6	0.0
K^{+}	3.8 - 5.4	5.0
PO_4^{--}	1.6 - 2.7	3.0
Mg^{++}	1.6 - 2.2	3.0
SO_4^{--}	.7 - 1.5	1.0
Dissolved Gases (mm Hg)		
O_2	0. - 40.	40. ± 20.
CO_2	45.	40. ± 20.
Electrical Voltages (mv)		
Nerve Activity	-90 to +50	
Muscle Activity	-85 to +100	Not Modelled.
Piezoelectric (bone)?		
Frequency of Load Application (cpm)		
	51 (level walking)	8500

* 1 milliequivalent/litre = mg/l x $\frac{\text{(valence)}}{\text{(molecular weight)}}$

Table 2. Mechanical Properties

TEST	TESTING MEDIUM	X-SECTION IN^2	GAUGE LENGTH CM	ELONGATION CM	ELONGATION %	AREA REDUCTION %	.02% YIELD LOAD KG	.02% YIELD STRENGTH PSI	ULTIMATE LOAD KG	ULTIMATE STRENGTH PSI
T1	AIR	.048	2.6	1.36	52	72	1600	73,500	1925	88,438
T2	AIR	.048	2.4	1.32	55	78	1600	73,500	1930	88,667
T3	AIR	.049	2.3	1.34	58	73	1625	73,122	1950	87,755
T4	AIR	.050	2.4	1.30	54	78	1620	71,440	1965	86,660
T5	RINGER'S(1)	.049	2.4	*	*	72	*	*	*	*
T6	RINGER'S(2)	.050	2.3	1.43	62	79	1620	71,440	2010	88,640
T7	RINGER'S(3)	.049	2.3	1.42	62	77	1600	72,000	1965	88,429
T8	RINGER'S(4)	.049	2.3	1.60	69	78	1580	71,102	1940	87,306

* Indicates recorder not functioning.

(1) pH = 7.7 pO_2 = 55 mm Hg pCO_2 = 57 mm Hg

(2) pH = 7.7 pO_2 = 46 mm Hg pCO_2 = 36 mm Hg

(3) pH = 7.5 pO_2 = 36 mm Hg pCO_2 = 36 mm Hg

(4) pH = 7.8 pO_2 = 39 mm Hg pCO_2 = 32 mm Hg

Table 3. Average Mechanical Properties.

TESTS	ELONGATION %	AREA REDUCTION %	.02% YIELD STRENGTH PSI	ULTIMATE STRENGTH PSI
T1 to T4 (AIR)	54.75	75.25	72,891	87,880
T5 to T8 (RINGER'S)	64.33	76.50	71,847	88,125
ALL	58.86	75.88	72,443	87,987

Table 4. Results of Fatigue Tests Conducted in Air.

MAXIMUM ALTERNATING STRESS KSI	TEST NUMBER	SPECIMEN LIFE KC
66.7	12	2,347
66.7	13	5,000 +
66.7	16	4,097 +
66.7	67	5,000 +
70.7	61	139
70.7	69	282
70.7	70	430
70.7	71	184
70.7	72	250
76.	66	800
76.	73	98
76.	74	356
76.	75	164
76.	77	184
80.	14	91
80.	15	70
80.	17	68
80.	18	81

+ Removed from testing apparatus unbroken.

Table 5. Results of Fatigue Tests Conducted in Distilled Water.

MAXIMUM ALTERNATING STRESS	TEST NUMBER	pO_2	pCO_2	pH	SPECIMEN LIFE
KSI		MM HG	MM HG		KC
66.7	55	62	43	5.5	2,497
66.7	57	69	65	5.4	5,000 +
76.	43	44	36	5.4	86
76.	44	53	32	5.4	89
76.	45	58	31	5.2	80
76.	48	50	32	5.4	172
80.	41	60	57	4.9	59
80.	42	42	44	5.2	69

\+ Removed from testing apparatus unbroken.

Table 6. Results of Fatigue Tests Conducted in Ringer's Solution.

MAXIMUM ALTERNATING STRESS KSI	TEST	pO_2 MM HG	pCO_2 MM HG	pH	SPECIMEN LIFE KC
60.	39	49.	49	7.6	5,000 +
60.	40	90	40	8.0	5,000 +
66.7	30	72	47	7.4	268
66.7	32	52	43	7.5	222
66.7	33	50	34	7.6	142
70.7	34	59	46	7.5	111
70.7	35	36	46	7.6	123
70.7	36	48	35	7.6	280
70.7	52	51	28	8.0	127
76.	37	47	44	7.4	50
76.	38	60	32	7.6	57
76.	49	52	47	7.6	104
80.	21	100	35	7.5	45
80.	22	65	46	7.6	54
80.	23	50	20	7.2	47
80.	24	51	47	7.4	53
80.	25	28	20	7.7	50

+ Removed from testing apparatus unbroken.

Table 7. Application of Chauvenet's Criterion.

TESTING MEDIUM	MAXIMUM ALTERNATING STRESS	DATA GROUP	$\bar{X}$	S	X_e	C	C'*	ACCEPTABLE** ?
	KSI	KC	KC	KC	KC			
AIR	76.	800;356;184;164;98	320.40	284.52	800	1.69	1.64	NO
AIR	76.	356;184;164;98	200.50	110.00	356	1.41	1.53	YES
AIR	70.7	436;282;250;184;139	258.20	113.97	436	1.56	1.64	YES
WATER	76.	172;89;86;80	106.75	43.67	172	1.49	1.53	YES
RINGER'S	70.7	280;127;123;111	160.25	80.12	280	1.49	1.53	YES
RINGER'S	66.7	5000+;268;222;142	2138.3	3855.5	5000+	1.50	1.64	YES

* From Basic Statistical Methods for Engineers and Scientists by Neville and Kennedy (32).

** If C is greater than C', outlier can be rejected with 95% confidence.

Table 8. Summary of Statistical Analyses.

MAXIMUM ALTERNATING STRESS	TESTING MEDIUM AIR			DISTILLED WATER			RINGER'S SOLUTION		
KSI	$\bar{X}$ KC	(TESTS)	σ KC	$\bar{X}$ KC	(TESTS)	σ KC	$\bar{X}$ KC	(TESTS)	σ KC
60.	-	-	-	-	-	-	5000+	(2)	-
66.7	4130	(4)	1020	3749	(2)	-	2138.3	(4)	2074.33
70.7	258.2	(5)	83.15	-	-	-	160.25	(4)	69.39
76.	200.5	(4)	95.25	106.75	(4)	37.81	70.33	(3)	23.98
80.	77.5[a]	(4)	9.23	64.[b]	(2)	5.	49.80[a,b]	(5)	3.43

\+ All specimens in this data group removed unbroken at 5 millions cycles.

a-a A statistically significant difference at the 99% confidence level exists between these data group means.

b-b A statistically significant difference at the 95% confidence level exists between these data group means.

Table 9-A. Load Cell Calibration.

LOAD KG	INDICATED STRAIN μ IN/IN			
	TRIAL 1	CHANGE	TRIAL 2	CHANGE
0	-1218	0	-1200	0
100	-1193	25	-1174	26
200	-1170	23	-1150	24
300	-1145	25	-1125	25
400	-1122	23	-1100	25
500	-1098	24	-1075	25
600	-1074	24	-1051	24
0	-1218	-144	-1198	-147

$$1\ \mu\ in/in = \frac{100 \times 2.205}{(147 + 144)/12} = 9.06\ lb.$$

Table 9-B. Amsler Vibraphore Verification.

LOAD LB	INDICATED STRAIN μ IN/IN					
	TRIAL 1	TRIAL 2	TRIAL 3	TRIAL 4	ABSOLUTE AVERAGE	TRUE LOAD LB
0	-1200	-1200	-1200	-1200	0.	0.
200	-1177	-1178	-1178	-1178	22.25	201.6
400	-1156	-1156	-1155	-1156	44.25	400.9
600	-1133	-1134	-1132	-1134	66.75	604.8
800	-1109	-1109	-1108	-1109	91.25	826.7
1000	-1086	-1087	-1087	-1087	113.25	1026.0
1200	-1065	-1064	-1064	-1064	135.75	1229.6

Error at indicated load of 1000 lb. + 2.6%.

Error at indicated load of 1200 lb. + 2.5%.

Table 10. ASTM Specification for 316L Stainless Steel Composition.

ELEMENT	ASTM REQUIREMENT (34)	WEIGHT PERCENT EXPERIMENTAL STOCK CONTENT
Carbon	.03 max.	.04 *
Manganese	2.0 max.	1.7
Phosphorus	.03 max.	**
Sulfur	.03 max.	**
Silicon	.75 max.	**
Chromium	17.0 - 20.0	17.78
Nickel	10.0 - 14.0	12.50
Molybendum	2.0 - 3.0	1.96
Iron	Balance	**

* Courtesy of Warnock-Hersey Professional Services Ltd.

** Not analyzed.

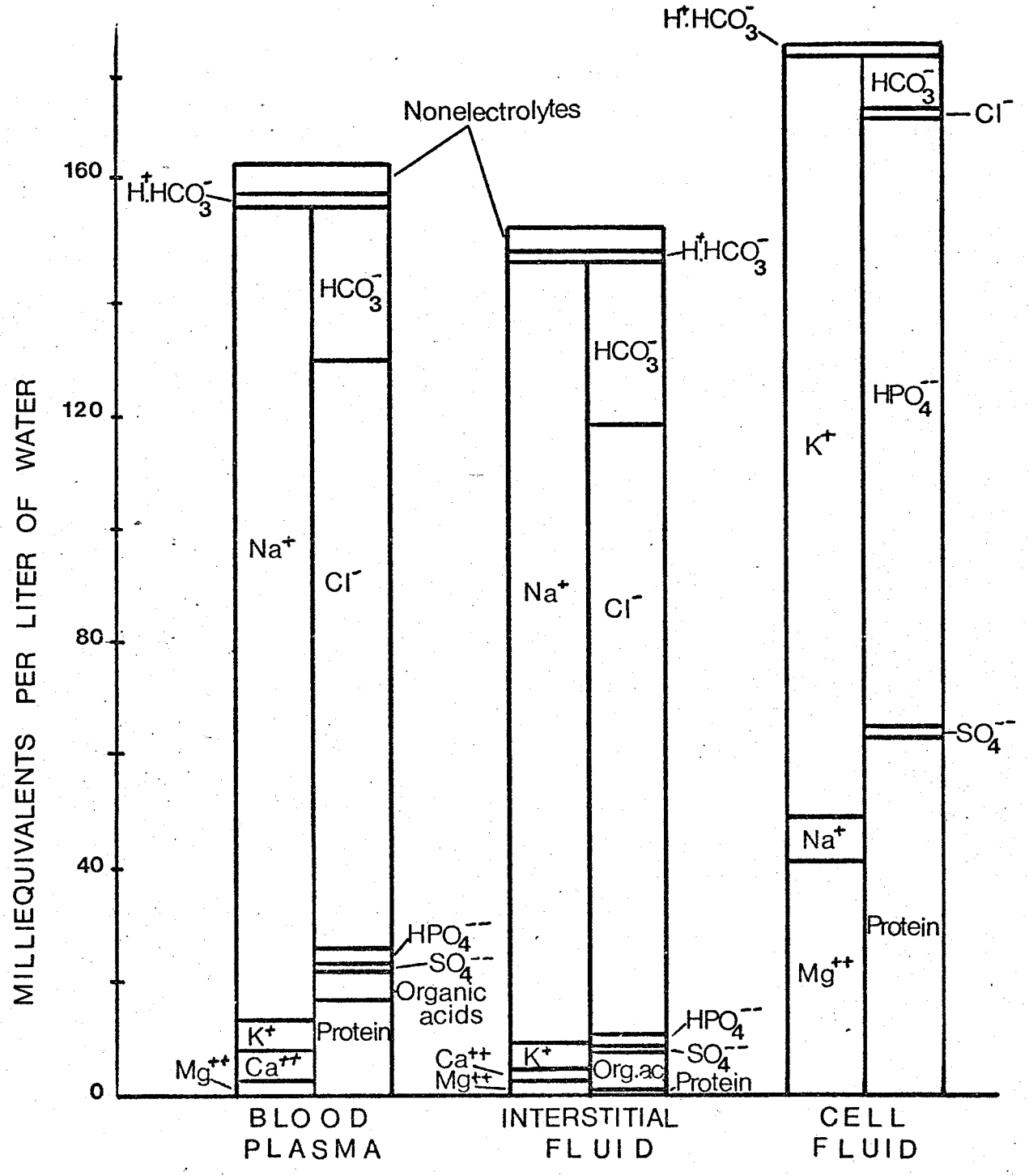

Figure I. Composition of intracellular and extracellular fluids. After Guyton (22).

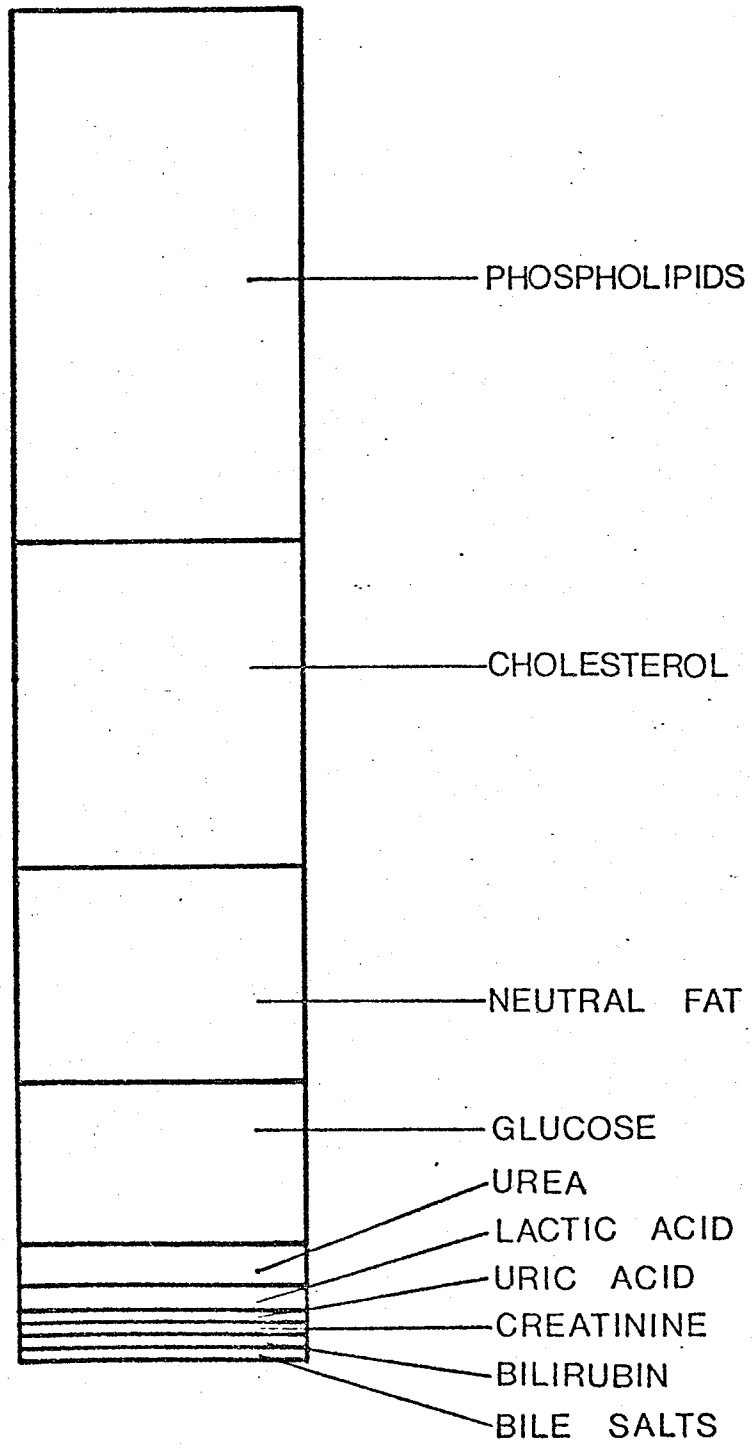

Figure 2. Relative abundance by weight of the nonelectrolytes of extracellular fluid. After Guyton (22).

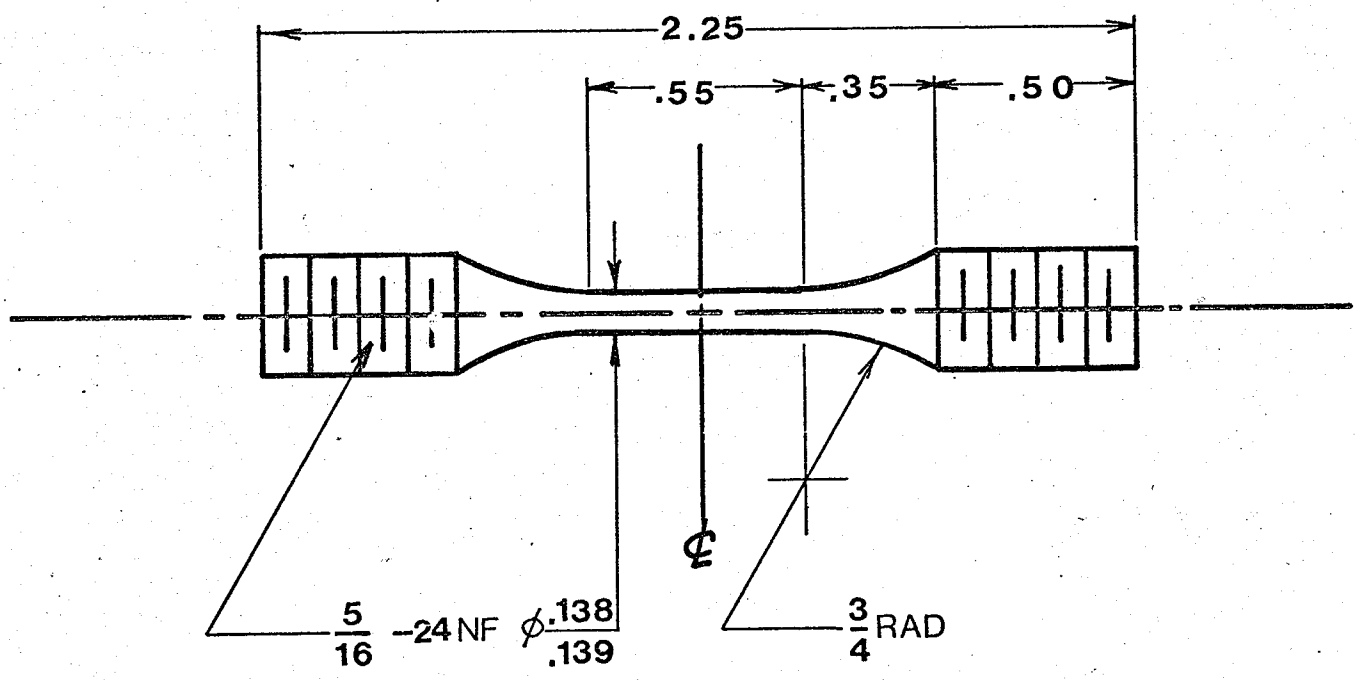

Figure 3. Fatigue specimens.

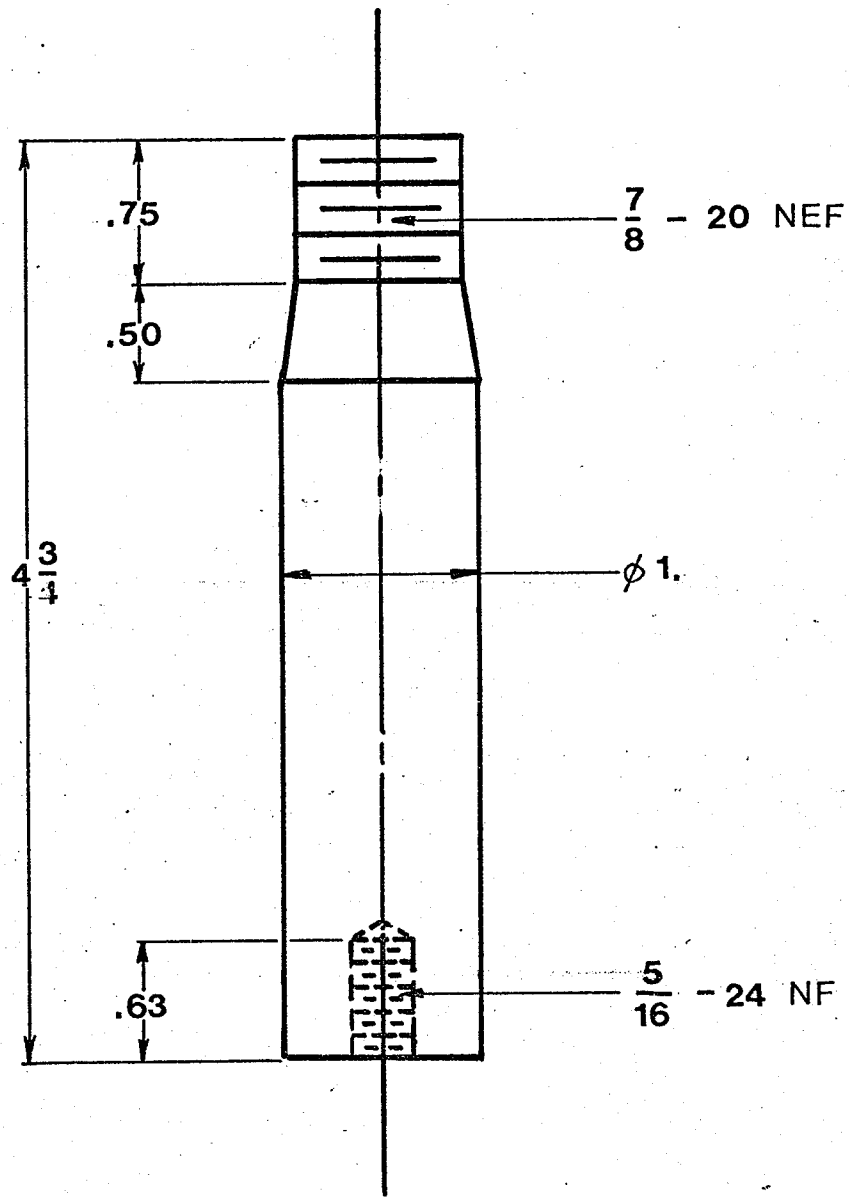

Figure 4. Fatigue specimen adaptors.

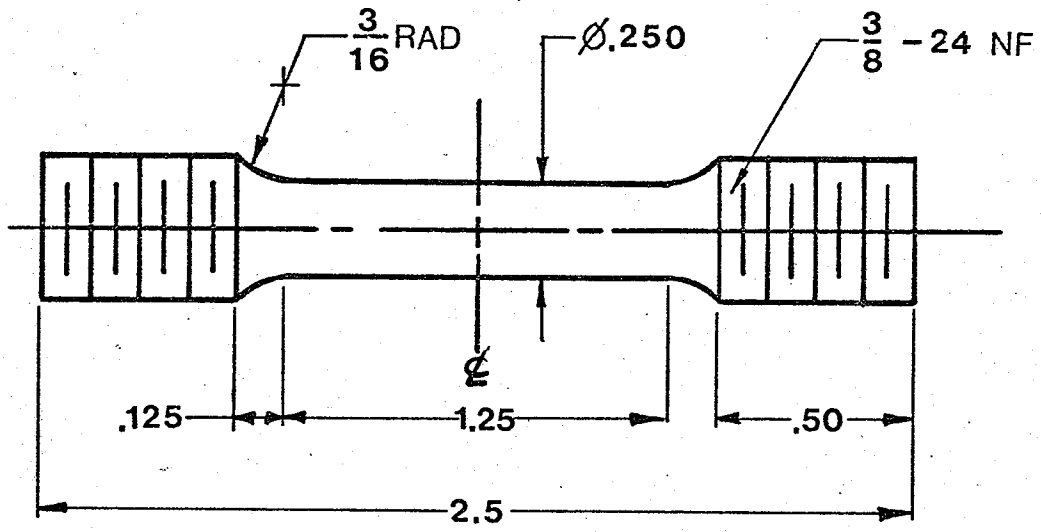

Figure 5. Tensile specimens.

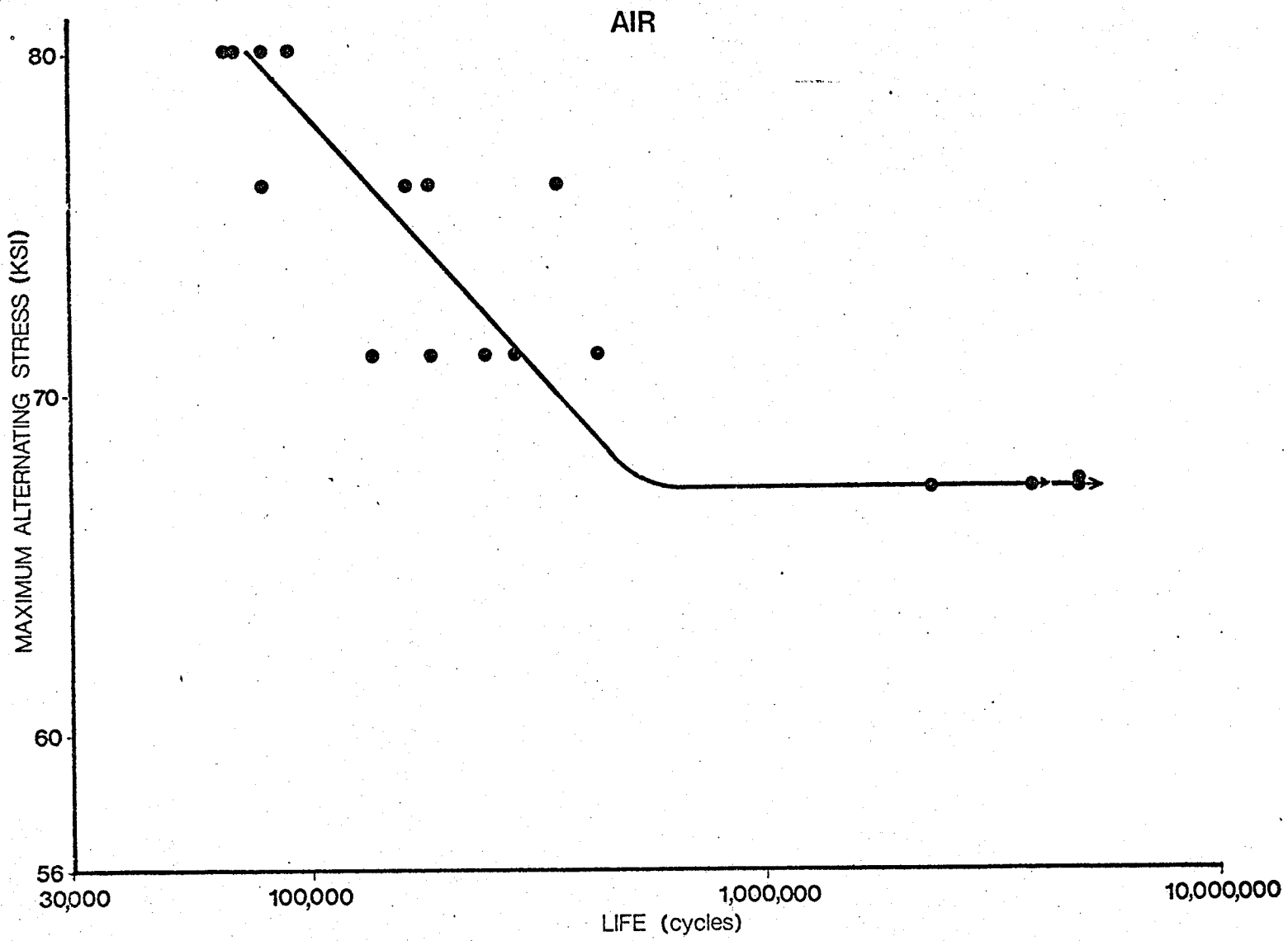

Figure 6. Results of tests conducted in air.

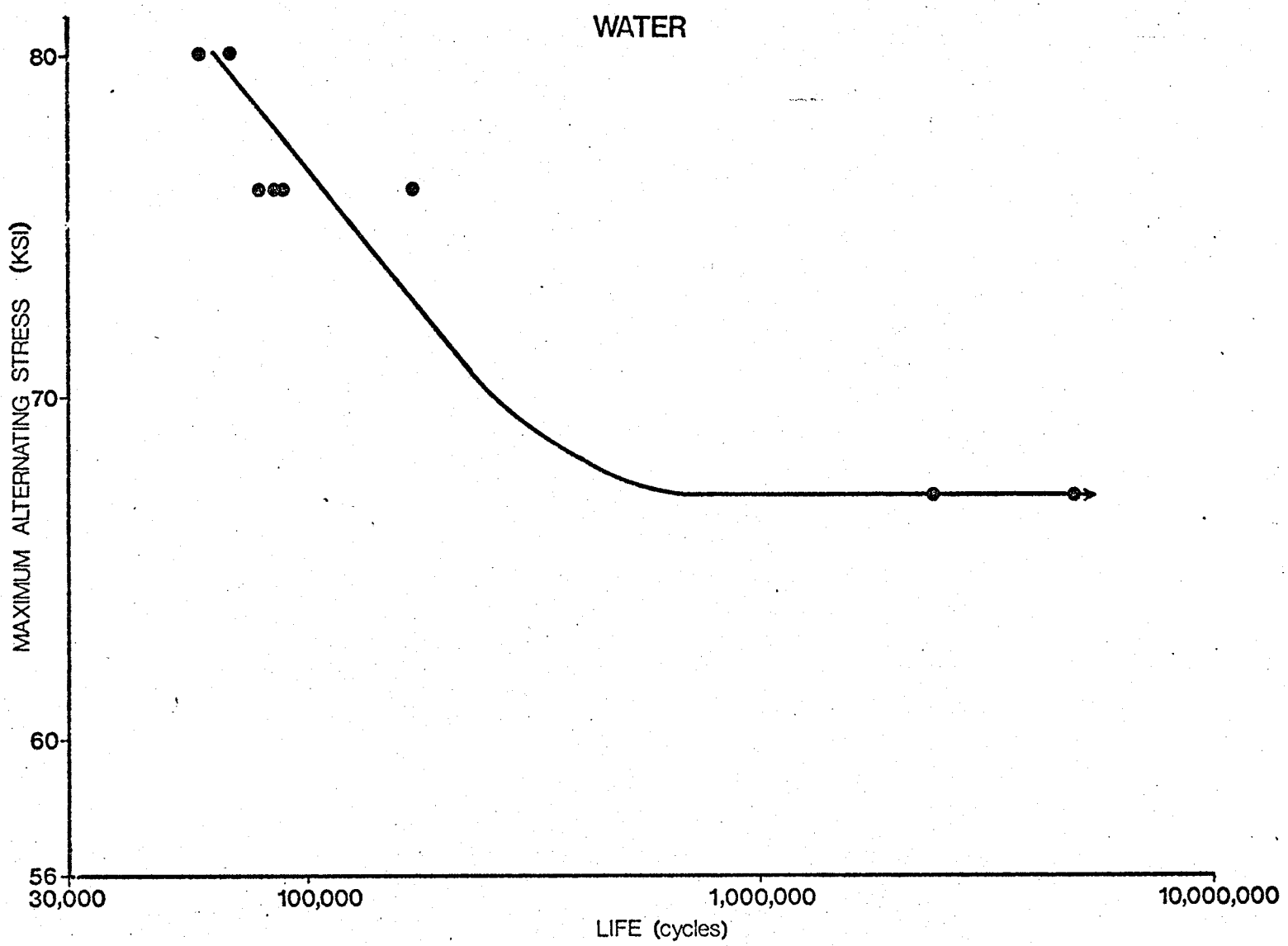

Figure 7. Results of fatigue tests conducted in water.

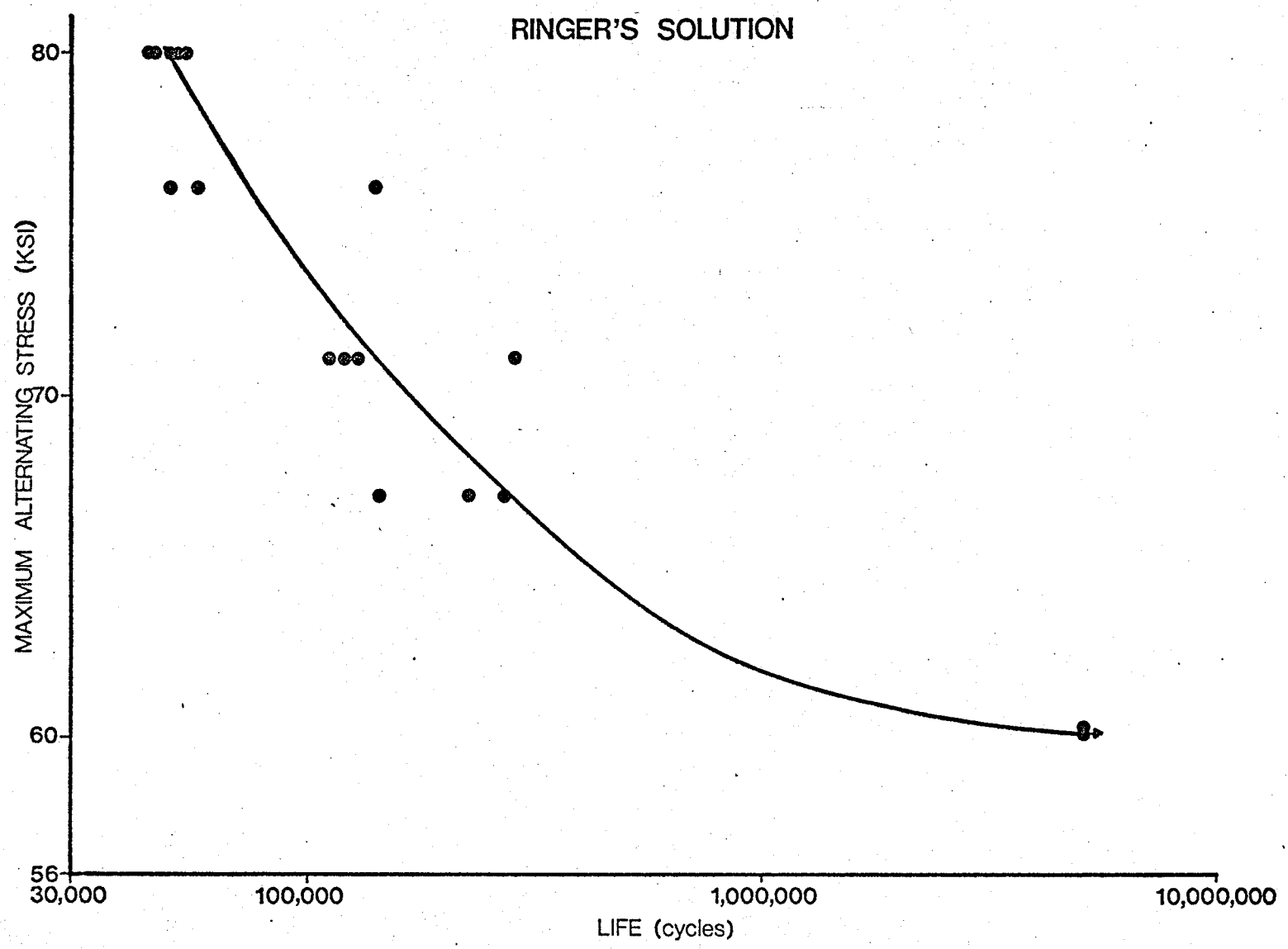

Figure 8. Results of fatigue tests conducted in Ringer's solution.

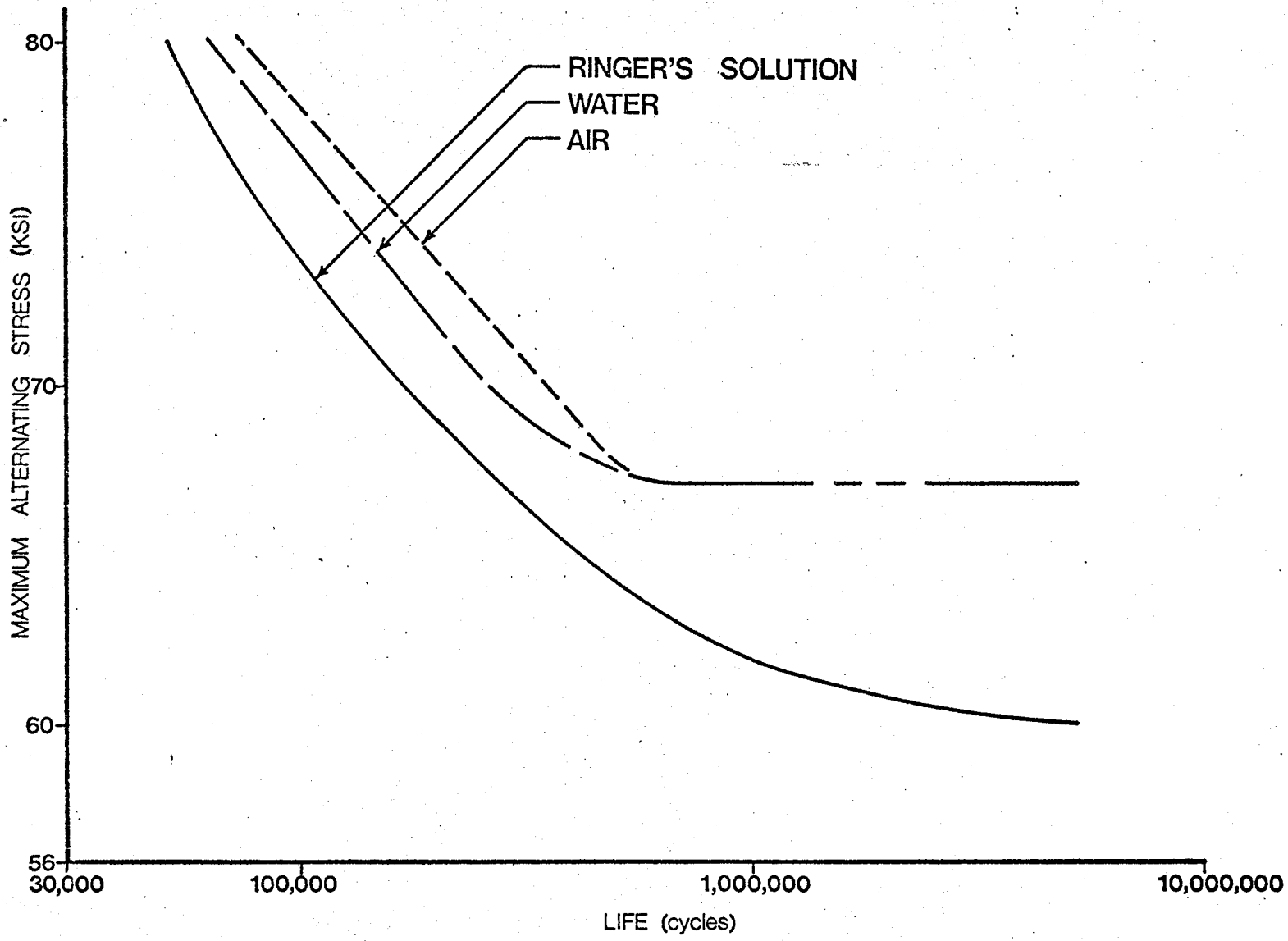

Figure 9. Comparison of fatigue test results.

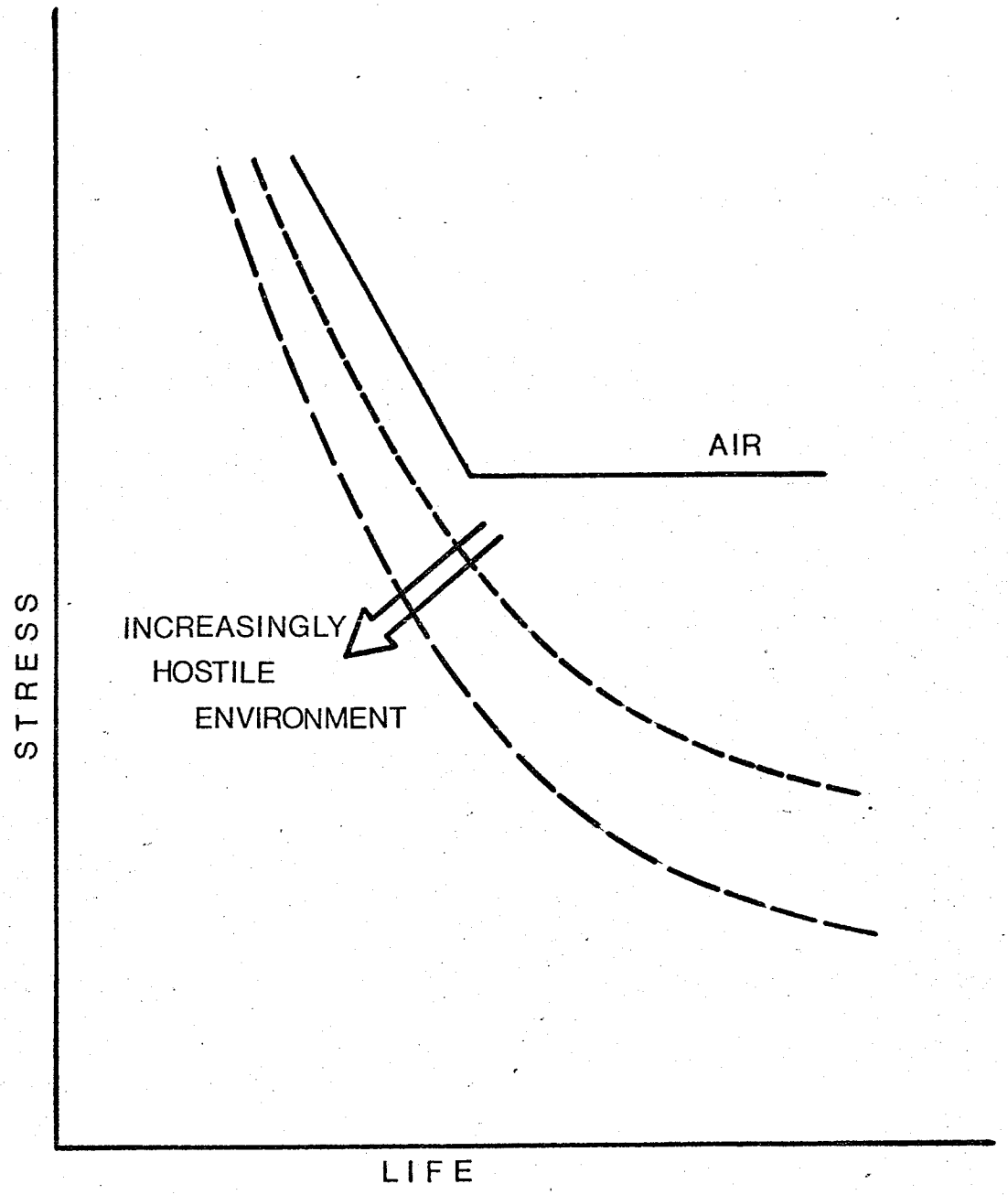

Figure IO. Ferrous metals corrosion-fatigue S-N diagram.

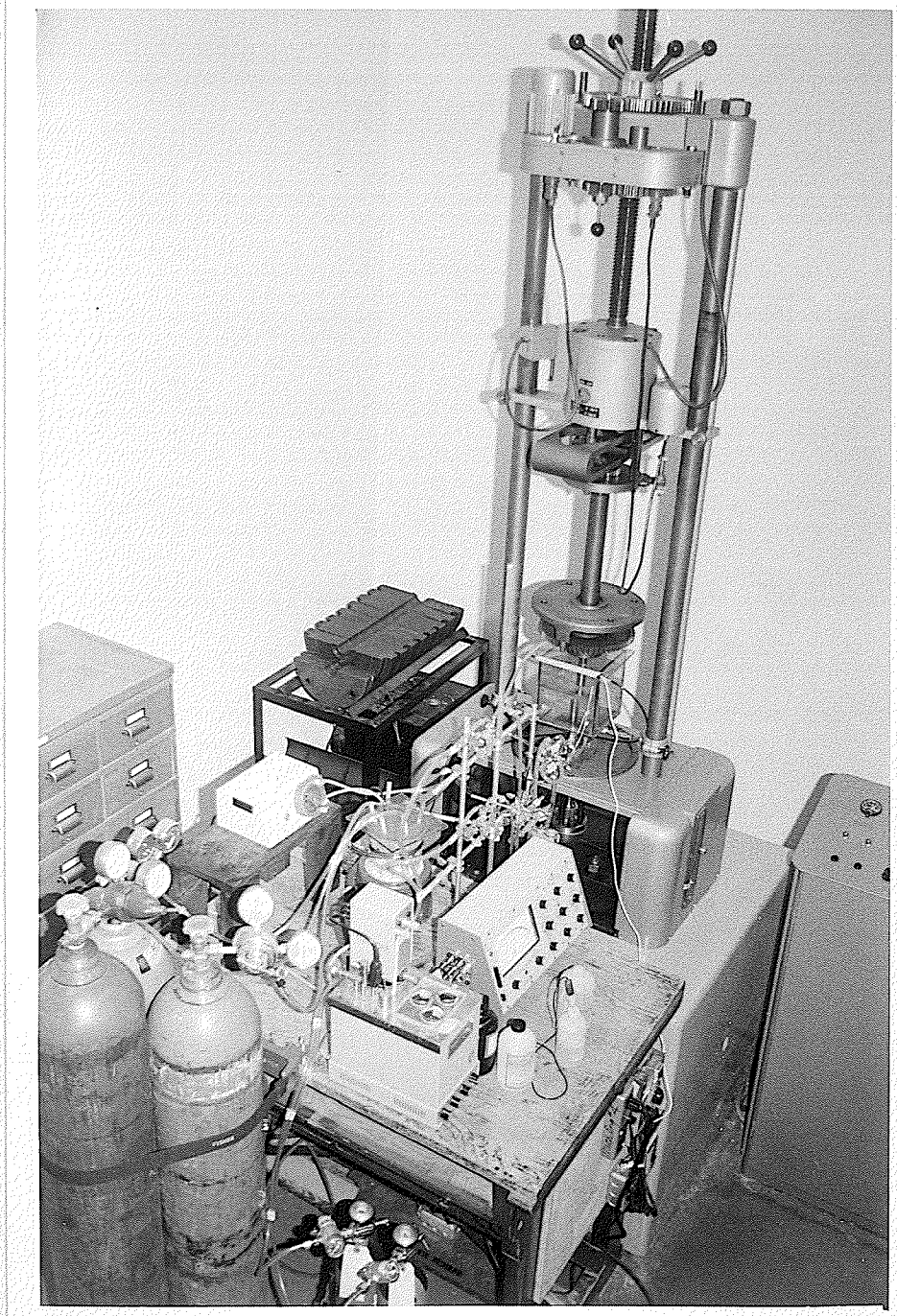

Photo 1. Apparatus arranged for liquid environment tests. The Amsler Vibraphore is in the background.

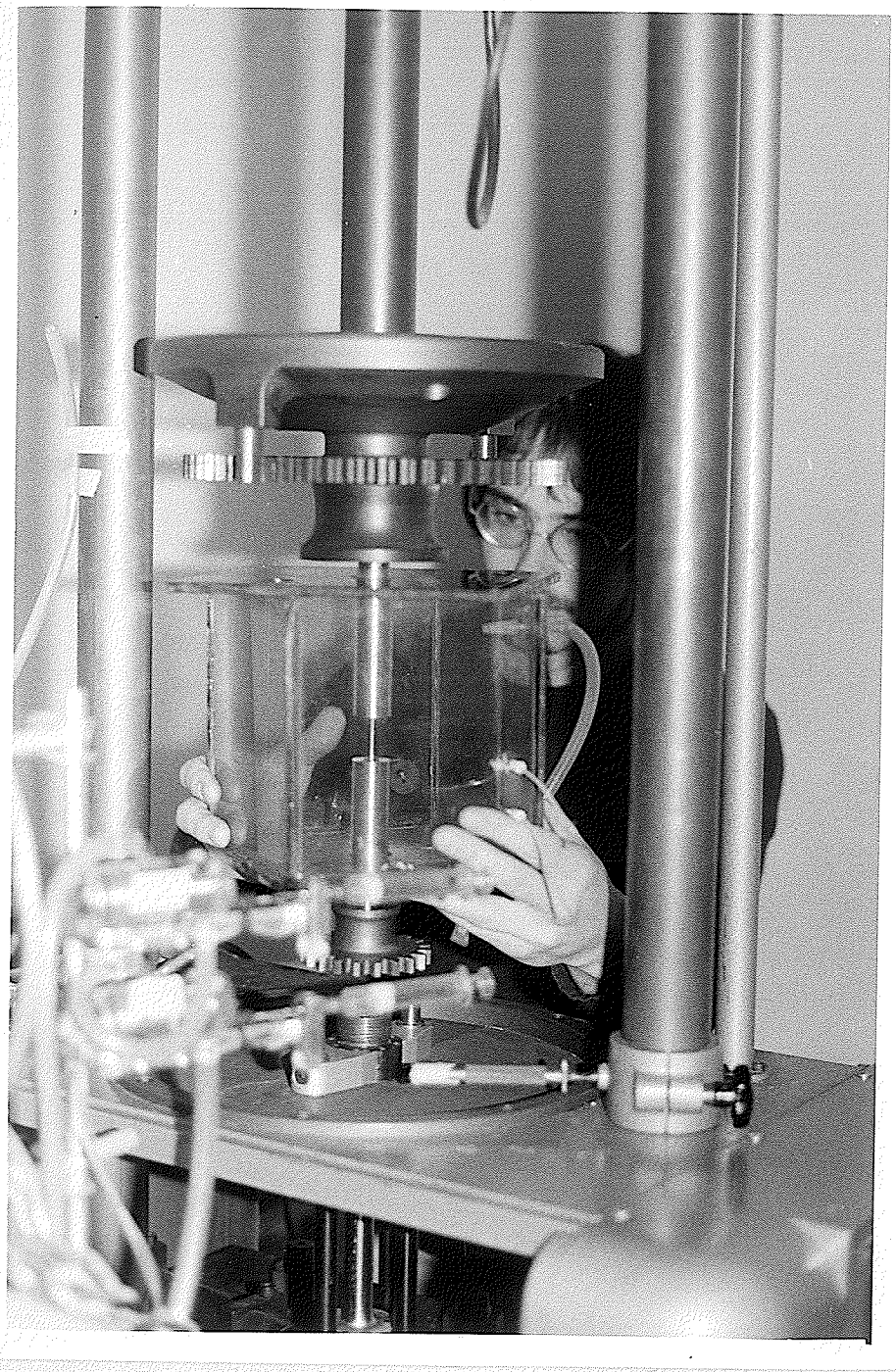

Photo 2. Environmental cell being positioned prior to testing.

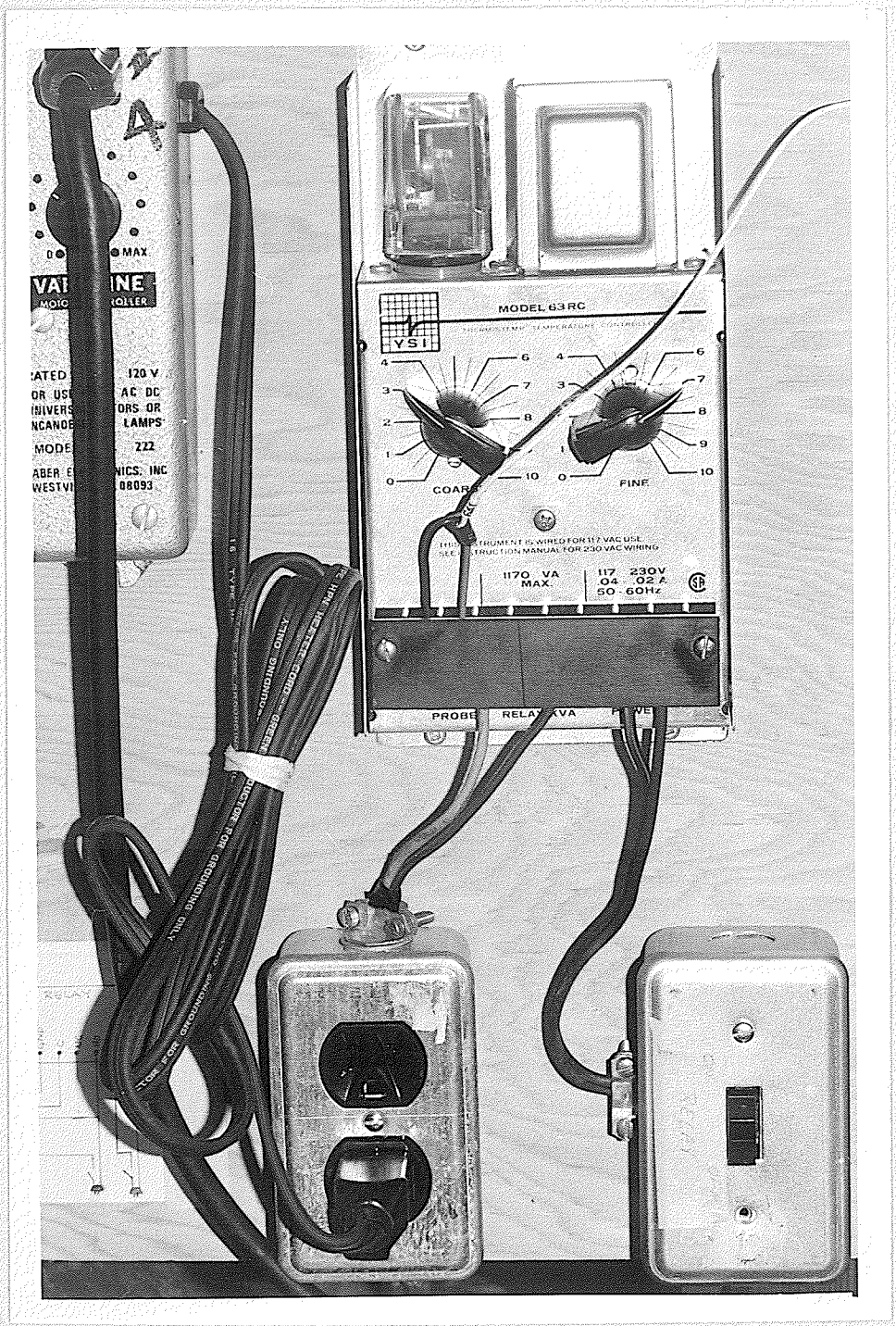

Photo 3. Temperature control equipment. The wire in the top right corner is the lead from the thermoprobe.

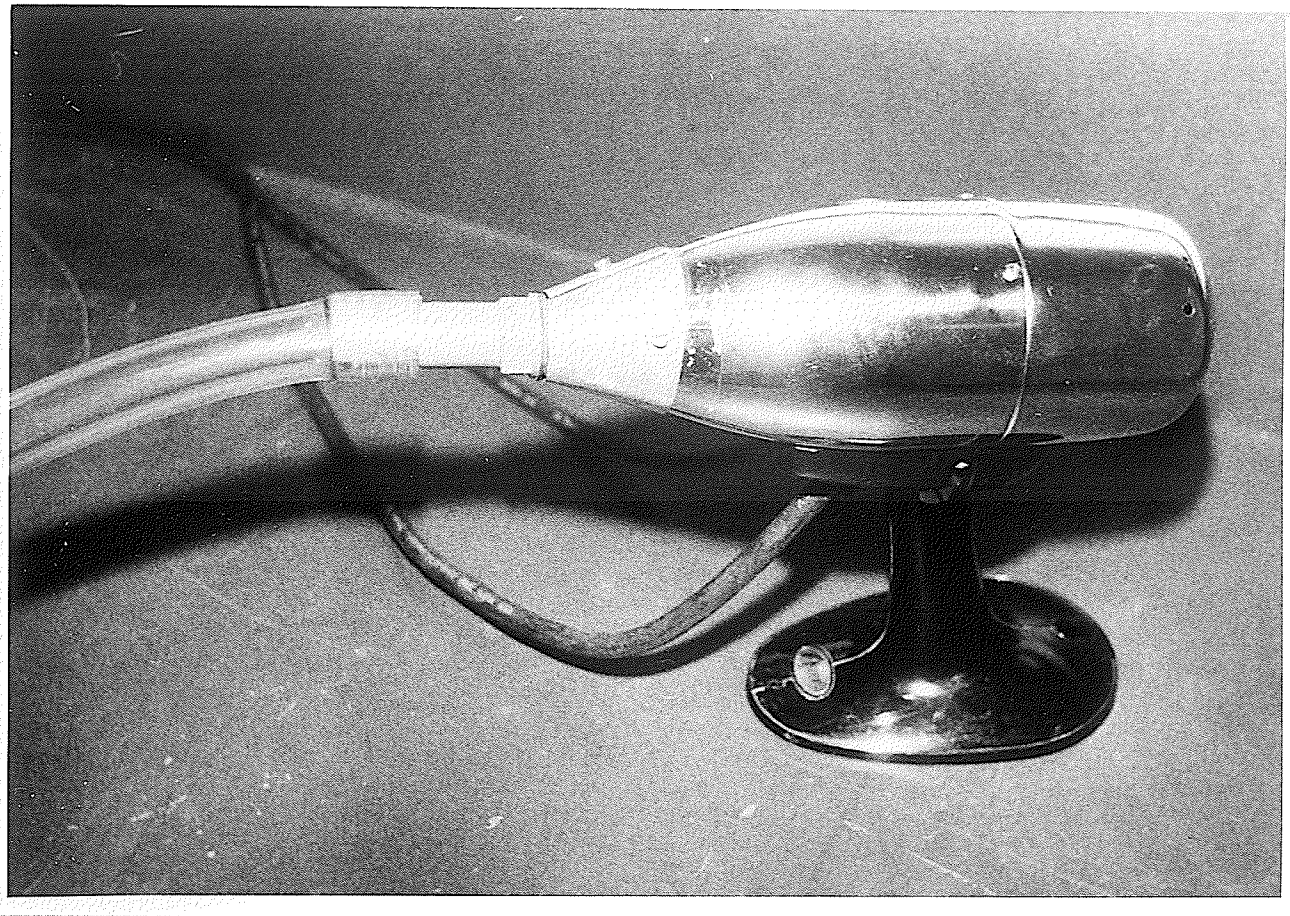

Photo 4. Air heater-fan.

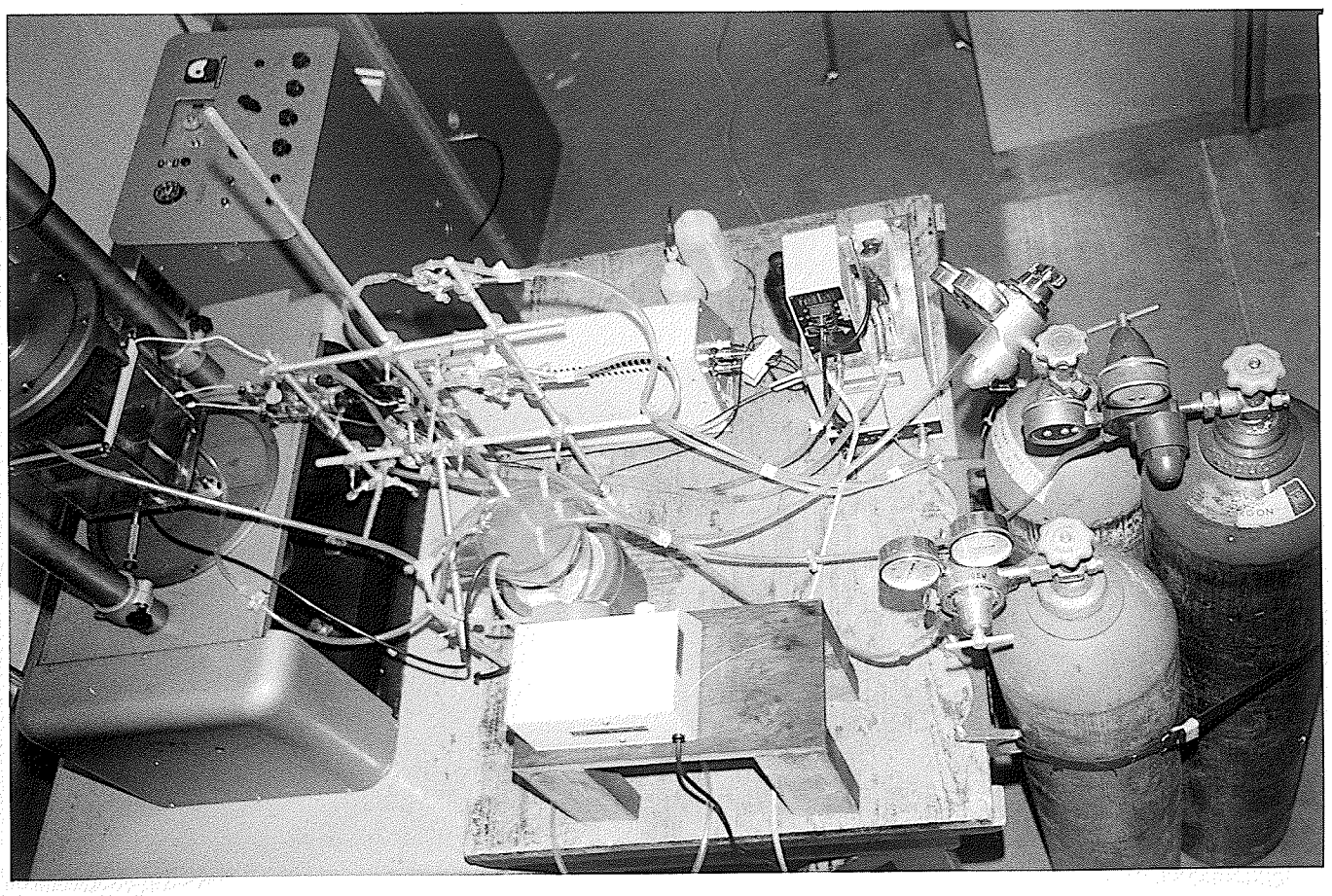

Photo 5. Apparatus view from above. The heating chamber containing the airstones is in the middle of the table.

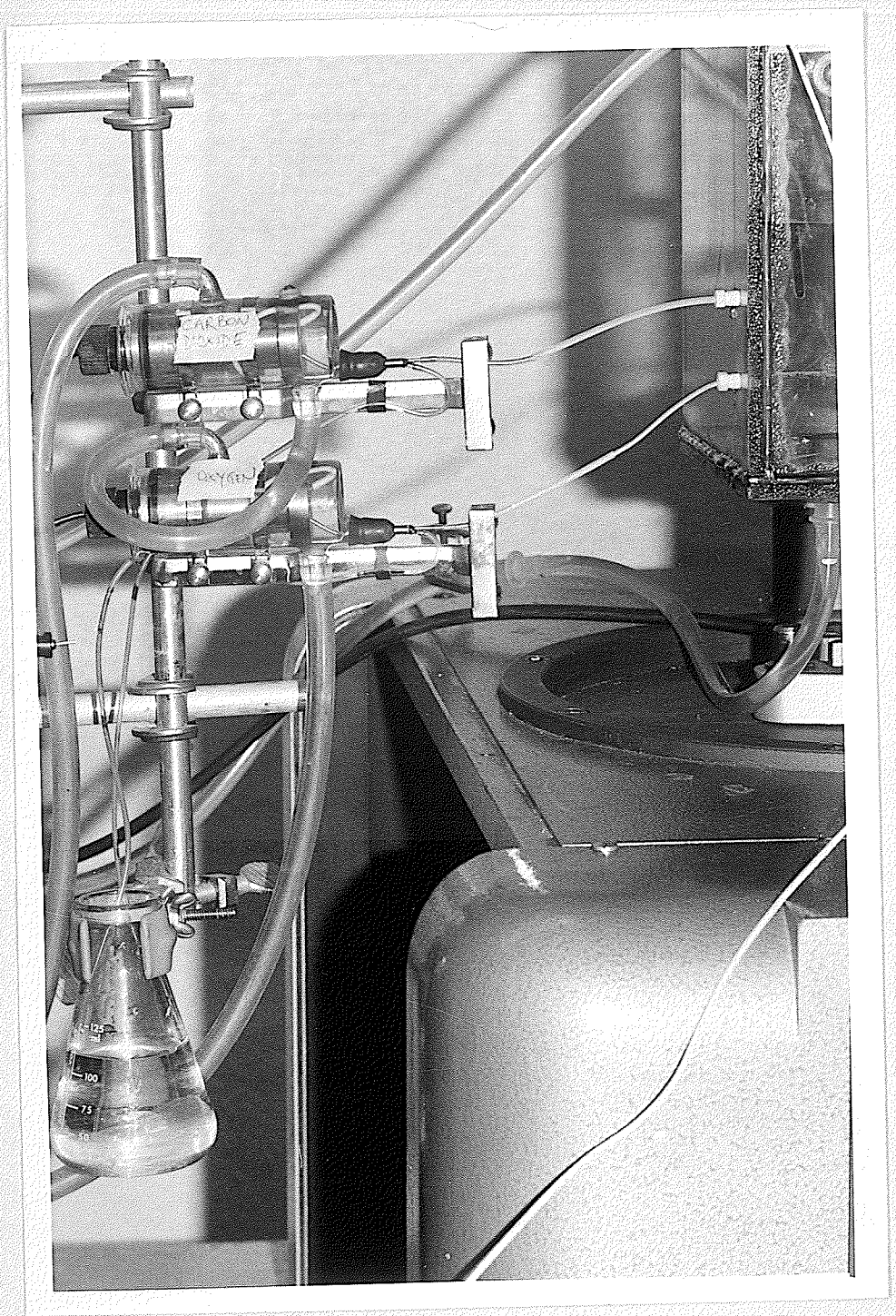

Photo 6. Leads from pO_2 and pCO_2 electrodes to environmental cell.

Photo 7. Microstructure of specimen 33. Etchant: equal parts HCl, HNO_3, and glycerine. Magnification: 100x.

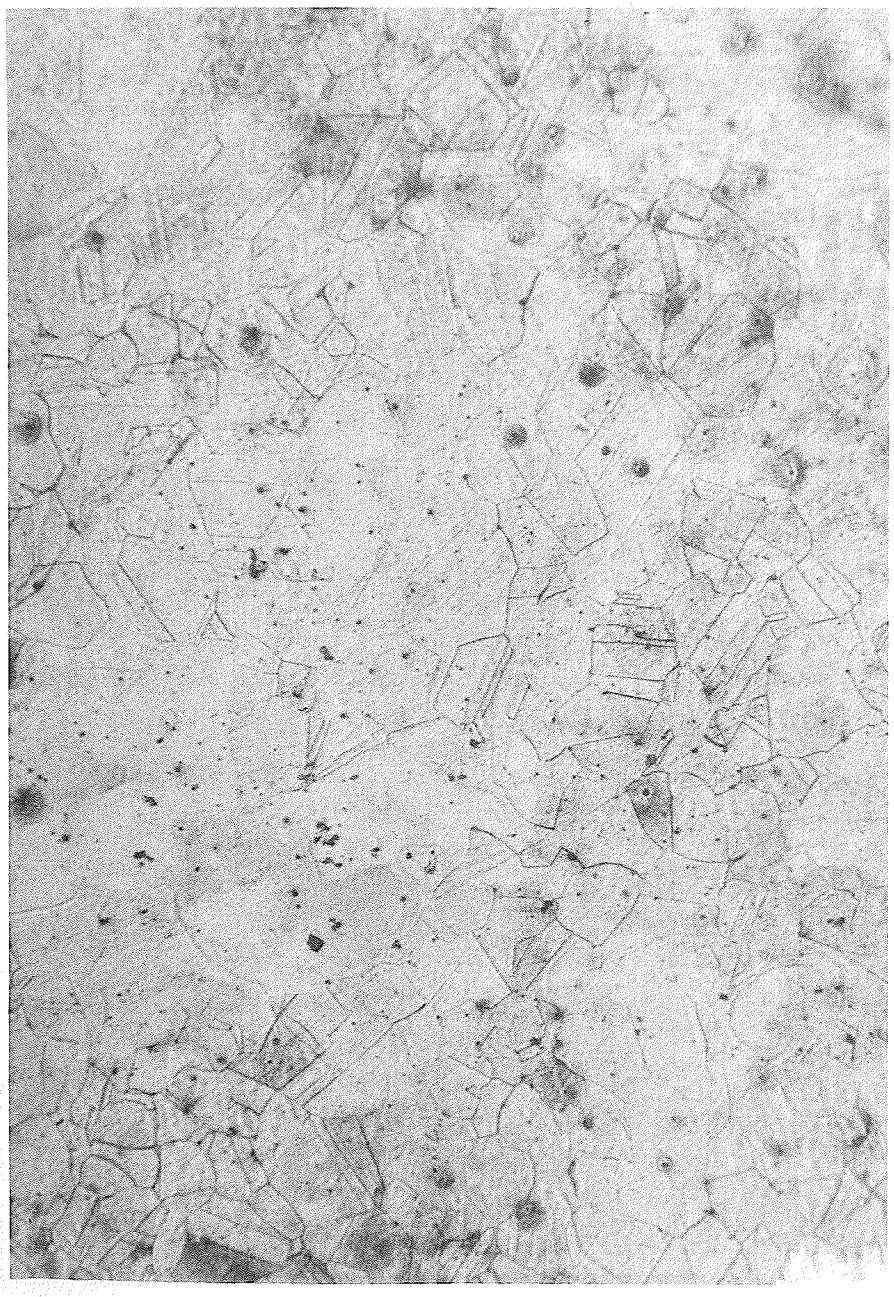

Photo 8. Microstructure of specimen 57. Etchant: equal parts HCl, HNO_3, and glycerine. Magnification: 100x.

Photo 9. Microstructure of specimen 61. Etchant: equal parts HCl, HNO_3, and glycerine. Magnification: 100x.

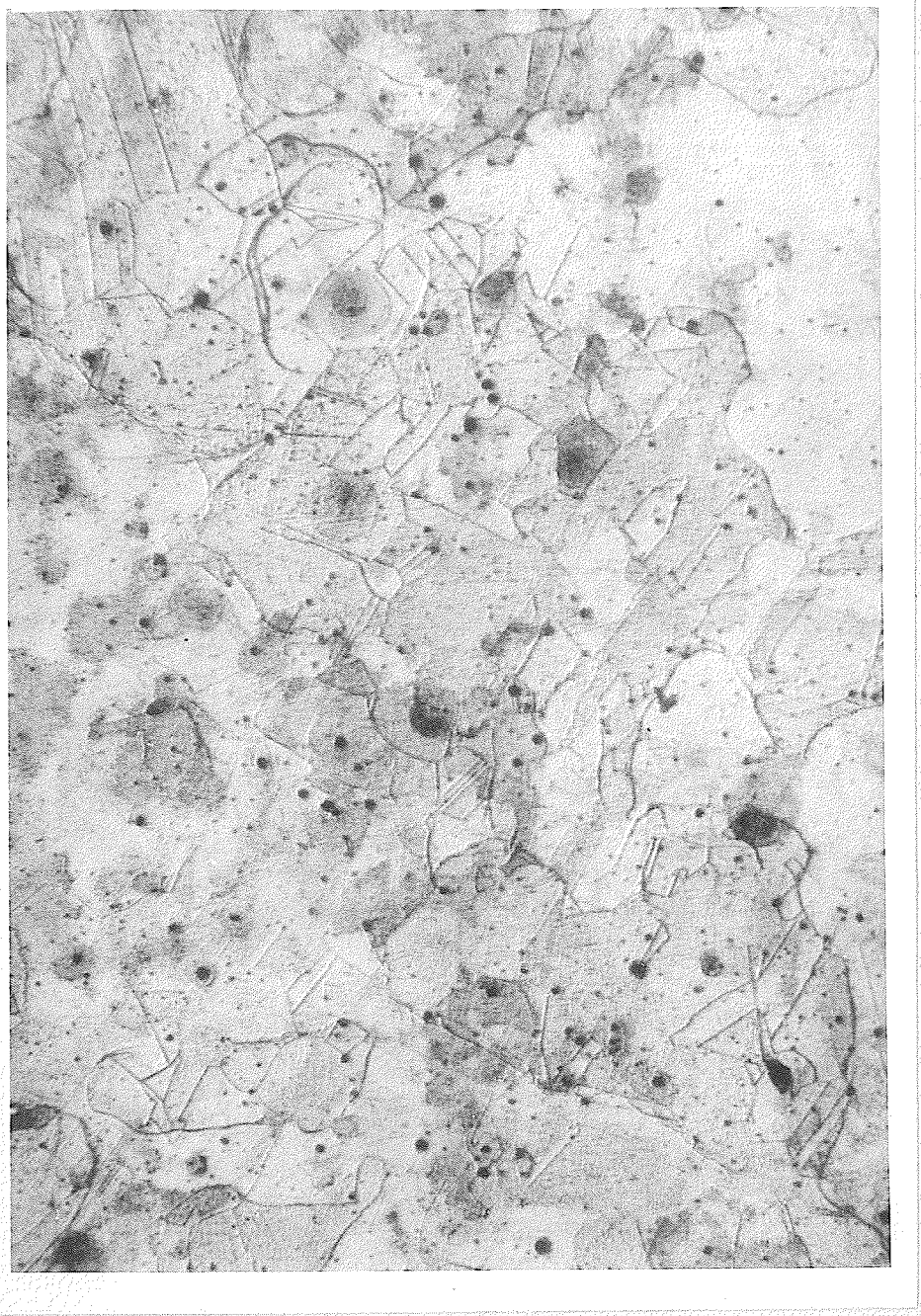

Photo 10. Microstructure of specimen 71. Etchant: equal parts HCl, HNO_3, and glycerine. Magnification: 100x.

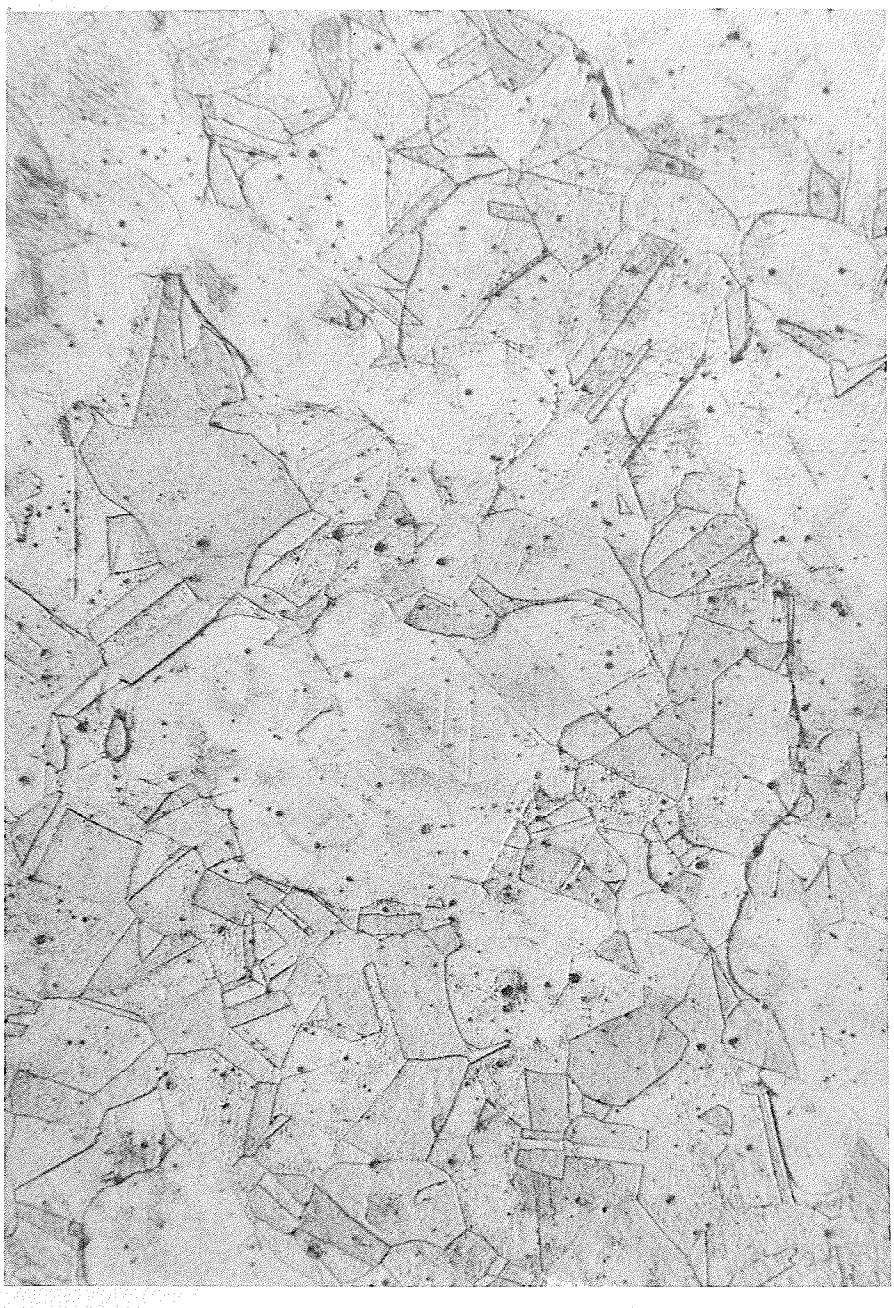

Photo 11. Microstructure of specimen 77. Etchant: equal parts HCl, HNO_3, and glycerine. Magnification: 100x.

REFERENCES

[1] Venable, C.S. and Stuck, W.G., The Internal Fixation of Fractures, Charles C. Thomas, Springfield, Illinois, 1947.

[2] Lane, W.A., The Operative Treatment of Fractures, Medical Publishing Co., London, 1914.

[3] Williams, D.F. and Roaf, R., Implants in Surgery, W.B. Saunders Co., London, 1973.

[4] Large, M., Krupp Steel Wire as a Bone Suture Material, Zeitschrift für Orthopädische Chirurgie, 47, 520, 1962.

[5] Cahoon, J.R. and Paxton, H.W., Metallurgical Analysis of Failed Orthopedic Implants, J. Biomedical Materials Research, 2, p. 1, 1968.

[6] Colangelo, V.J., Corrosion Fatigue in Surgical Implants, J. Basic Engineering, ASME Trans. Series D, 91, 581, 1969.

[7] Colangelo, V.J. and Greene, N.D., Corrosion and Fracture of Type 316 SMo Orthopedic Implants, J. Biomedical Material Research, 3, p. 247, 1969.

[8] Brettle, J. and Hughes, A.N., A Metallurgical Examination of Surgical Implants which gave Failed in Service, Injury, 2, p. 143, 1970.

[9] Hughes, A.N. and Jordan, B.A., Metallurgical Observations on some Metallic Surgical Implants which Failed In Vivo, J. Biomedical Materials Research, 6, p. 33, 1972.

[10] Weinstein, A., Amstutz, H., Pavon, G., and Franceschini, V., Orthopedic Implants: A Clinical and Metallurgical Analysis, J. Biomedical Materials Research Symposium, 4, 297, 1973.

[11] Scales, J.T., Winter, G.D., and Shirley, H.T., Corrosion of Orthopedic Implates: Screws, Plates, and Femoral Nail-plates, J. Bone and Joint Surgery, 41B, 810, 1959.

[12] Scales, J.T., Winter, G.D., and Shirley, H.T., Corrosion of Orthopedic Implants: Smith-Peterson Type Nails, British Medical J., 2, p. 478, 1961.

[13] Cohen, J., Performance and Failure in Performance of Surgical Implants in Orthopedic Surgery, J. Materials, 1, 354, 1966.

[14] Rama Char, T.L., Electrochemical Aspects of Corrosion Fatigue, Corrosion Prevention and Control, 19, # 5, p. 8, October 1972.

[15] Cahoon, J.R., Chaturvedi, M.C., and Tennese, W.W., Corrosion Studies on Metallic Implant Materials, Medical Instrumentation, 7, # 2, p. 131, March-April 1973.

[16] Laing, P.G., and O'Donnell, J.M., The Engineering Design of Hip Nails and Development of the H-Beam Nail, Surgery, Gynecology, and Obstetrics, 112, p. 567, May 1961.

[17] Grover, H.J., Metal Fatigue in Some Orthopedic Implants. J. Materials, 1, p. 413, 1966.

[18] Cohen, J., Corrosion Testing of Orthopedic Implants, J. Bone and Joint Surgery, 41A, p. 307, 1962.

[19] Wheeler, K.R. and James, L.A., Fatigue Behaviour of Type 316 Stainless Steel under Simulated Body Conditions, J. Biomedical Materials Research, 5, p. 267, 1971.

[20] Conway, J.B., Berling, J.T., and Stentz, R.H., Rep. GEMP-702, G.E.C., Cincinnati, 1969.

[21] Brettle, J., A Survey of the Literature on Metallic Surgical Implants, Injury, 2, # I, p. 26, 1970.

[22] Guyton, A.C., Textbook of Medical Physiology, 4th Edition, W.B. Saunders Co., Philadelphia, 1971.

[23] Crouch, J.E., Functional Human Anatomy, 2nd Edition, Lea and Febiger, Philadelphia, 1972.

[24] Chafee, E.E. and Greisheimer, E.M., Basic Physiology and Anatomy, 2nd Edition, J.B. Lippincott Co., Philadelphia, 1969.

[25] Murray, C.R., The Timing of the Healing Process, J. Bone and Joint Surgery, 23, p. 598, 1941.

[26] Crimmins, D.S., The Selection and Use of Metals for Surgical Implants, J. Metals, 21, p. 38, 1969.

[27] Laing, P.G., Compatibility of Biomaterials, The Orthopedic Clinics of North America, p. 249, April 1973.

[28] Morral, F.R., Cobalt Alloys as Implants in Humans, J. Materials, 1, p. 384, 1966.

[29] Trottler, M., Bowman, G.E., and Peterson, R.R., Densities of Bones of White and Negro Skeletons, J. Bone and Joint Surgery, 42A, p. 50, 1960.

[30] Zarek, J.M. and Evans, E.J., Research in Biomechanics at the University of Surrey, Biomedical Engineering, 6, p. 70, February 1971.

[31] Bresler, B. and Frankel, J.P., ASME Trans., 72, p. 27, 1950.

[32] Neville, A.M. and Kennedy, J.B., Basic Statistical Methods for Engineers and Scientists, International Textbook Co., Scranton, 1964.

[33] Amsler, A.J. and Co., Instruction Manual for Amsler High Frequency Vibraphores, Schaffhausen, Switzerland.

[34] Annual Book of ASTM Standards, Part 46, Standard Specification for Stainless Steel Bars and Wire for Surgical Implants, Specification F55-71, p. 271, Philadelphia, 1974.

[35] Annual Book of ASTM Standards, Part 46, Standard Specification for Stainless Steel Bars and Wire for Surgical Implants (special quality), Specification F138-71, p. 300, Philadelphia, 1974.

[36] Fontana, M.G. and Greene, N.D., Corrosion Engineering, Wiley and Sons, New York, 1971.

[37] Madayag, A.F., Metal Fatigue: Theory and Design, John Wiley and Sons, New York, 1969.

[38] McAdam, D.J., Jr., Proc. ASTM, 26, p. 224, 1926.

[39] Crooker, T.W., and Lange, E.A., Corrosion Fatigue Crack Propagation of Some New High-Strength Steels, Trans. ASME, J. Basic Engineering, Series D, 91, p. 570, 1969.

[40] Endo, K. and Miyas, Y., Bull. Japan Soc. Mech. Eng., 1, p. 374, 1958.

[41] Laird, C. and Duquette, D.J., Mechanisms of Fatigue Crack Nucleation, from Corrosion Fatigue: Chemistry, Mechanics, and Microstructures, O. Devereux, A.J. McEvily, and R.W. Stahle, editors, NACE, Houston, 1972.

[42] Karpenko, G.V., Deyaki Pitanhya Fiz. Khim. Mechan. Metal. Akad. Nauk RSR, Inst Machinoznasta Ta Avtomatik, p. 47, 1958.

[43] Plumbridge, W.J., Review: Fatigue-crack Propagation in Metallic and Polymeric Materials, J. Materials Science, 7, p. 939, 1972.

[44] Laird, C. and Krause, A.R., Int. J. Fracture Mechanics, 4, p. 219, 1968.

[45] Laird, C. and Smith, G., Phil. Mag., 8, p. 1945, 1963.

[46] Porter, J. and Levy, J.C., J. Institute of Metals, 89, p. 86, 1960.

[47] Kemsley, D.S., J. Institute of Metals, 85, p. 420, 1956.

[48] Forsyth, P.J.E. and Stubbington, C.A., Nature, 175, p. 767, 1955.

[49] Forsyth, P.J.E., Int. Conf. on Fatigue, Institute of Mechanical Engineers and ASME, Paper 6.5, 1956.

[50] Grosskreutz, J.C., Physica Status Solidi, 47, p. 2, 359, October 1971.

[51] Marcus, H.L., Williams, J.C. and Paton, N.E., The Influence of Gaseous Environments on Corrosion Fatigue, Corrosion Fatigue: Chemistry, Mechanics, and Microstructures, loc. cit.